THE EFFECT OF PROPPANT SIZE AND CONCENTRATION ON HYDRAULIC FRACTURE CONDUCTIVITY IN SHALE RESERVOIRS

A Thesis

by

ANTON NIKOLAEV KAMENOV

Submitted to the Office of Graduate Studies of
Texas A&M University
in partial fulfillment of the requirements for the degree of

MASTER OF SCIENCE

Approved by:

Chair of Committee,	Ding Zhu
Committee Members,	A. Daniel Hill
	Yuefeng Sun
Head of Department,	A. Daniel Hill

May 2013

Major Subject: Petroleum Engineering

ABSTRACT

Hydraulic fracture conductivity in ultra-low permeability shale reservoirs is directly related to well productivity. The main goal of hydraulic fracturing in shale formations is to create a network of conductive pathways in the rock which increase the surface area of the formation that is connected to the wellbore. These highly conductive fractures significantly increase the production rates of petroleum fluids. During the process of hydraulic fracturing proppant is pumped and distributed in the fractures to keep them open after closure. Economic considerations have driven the industry to find ways to determine the optimal type, size and concentration of proppant that would enhance fracture conductivity and improve well performance. Therefore, direct laboratory conductivity measurements using real shale samples under realistic experimental conditions are needed for reliable hydraulic fracturing design optimization.

A series of laboratory experiments was conducted to measure the conductivity of propped and unpropped fractures of Barnett shale using a modified API conductivity cell at room temperature for both natural fractures and induced fractures. The induced fractures were artificially created along the bedding plane to account for the effect of fracture face roughness on conductivity. The cementing material present on the surface of the natural fractures was preserved only for the initial unpropped conductivity tests. Natural proppants of difference sizes were manually placed and evenly distributed along the fracture face. The effect of proppant monolayer was also studied.

The results from the experimental study showed that poorly cemented natural fractures can provide effective flow paths. Unpropped hydraulic fractures have sufficient conductivity after removal of free particles and debris generated during the fracturing process. In the absence of proppant, the conductivity of displaced induced fracture is of one order of magnitude higher than the conductivity of an aligned fracture. Unpropped fracture conductivity is strongly affected by the degree of shear displacement and the amount of removed rock or cementing material. Propped fracture conductivity is weakly dependent on fracture surface roughness. Proppant is the major contributor to conductivity even at low areal concentrations. Propped fracture conductivity increases with larger proppant size and higher areal concentration. Proppant partial monolayer cannot maintain conductivity at elevated closure stress.

DEDICATION

I would like to dedicate this work to my loving parents, Lalka and Nikolay, my brother, Victor, my sister, Liana, my uncle, Valentin and my grandparents, Liliana and Anton who encouraged and supported me throughout the course of my college career.

ACKNOWLEDGEMENTS

I would like to thank Dr. Ding Zhu and Dr. Daniel Hill for the great opportunity to pursue my Master of Science degree in petroleum engineering under their supervision. Their guidance and encouragement helped me complete my study.

Next, I would like to thank Dr. Yuefeng Sun for being a member of my committee. I would like to thank John Maldonado, Zhang Junjing and Alissa Aris for their help, support, and contribution to the project.

I would like to thank the Crisman Institute for their financial support.

I would to thank the Harold Vance Department of Petroleum Engineering for giving me the wonderful opportunity to pursue my graduate degree in petroleum engineering.

NOMENCLATURE

A	Cross-sectional area (in^2)
h_f	Fracture height (in)
k_f	Facture permeability (md)
L	Length over pressure drop (in)
M	Molecular mass (kg/ kg mole)
$p1$	Upstream pressure (psi)
$p2$	Downstream pressure (psi)
R	Universal gas constant (J/mol K
T	Temperature (K)
v	Fluid velocity (ft/min)
W	Mass flow rate (kg/min)
z	Gas compressibility factor (dimensionless)
ρ	Fluid density (lbm/ft^3)
μ	Fluid Viscosity (cp)
Δp	Differential pressure over the fracture length (psi)
$k_f w_f$	Fracture conductivity (md-ft)

TABLE OF CONTENTS

LIST OF FIGURES

LIST OF TABLES

1. INTRODUCTION

1.1 Hydraulic fracturing in shale reservoirs

Shale reservoirs contain enormous quantities of hydrocarbon resources that can be commercially produced only by applying hydraulic fracturing stimulation techniques. The main objective of hydraulic fracturing is to bypass near-wellbore formation damage and create a high-conductivity fracture that communicates with a large surface area of formation. Well productivity is directly associated with fracture conductivity. During the process of hydraulic fracturing a specially engineered fluid is pumped into the reservoir at a very high pressure and rate. The fracture fluid typically carries proppant such as natural sand or ceramic grains of a particular size and concentration. The proppant is distributed in the fractures to keep them open after the operation is complete. Currently, the industry is seeking ways to determine the optimal proppant size and concentration to improve fracture treatment efficiency while minimizing the cost of treatments

Hydraulic fracturing with high-viscosity fluids gained popularity in 1947 soon after the first successful fracturing treatment with gasoline-based fracturing fluid. The guar-based cross-linked fracturing fluids were introduced in the late 1960s and were very successfully used in well stimulation of low-permeability formations. During the 1970s many Hugotan wells in Kansas were effectively stimulated with the so called "river fracs" where water and low sand concentrations were pumped at the rate of 200 to 300 bbl/min with a few gallons of friction reducer (Grieser et al., 2003). Hydraulic fracturing operations in the Mississippian age Barnett Shale of the Fort Worth basin

began in the 1980s. Early well stimulation treatments consisted of pumping moderate conventional cross-linked gel systems of approximately 300,000 gallons of fluid and 300,000 pounds of sand. During the following years these treatments became massive and involved the pumping of 750,000 gallons of fluid and up to 1.5 million pounds of proppant, typically sand (Schein et al., 2004). The polymer concentrations ranged from 30 to 50 pounds per 1000 gallons (Coulter et al., 2004).

In 1997 slickwater fracturing was introduced and later became the most popular well stimulation technique mainly because it reduced the potential for gel damage, lowered costs, and provided more complex fracture geometry which was evident from microseismic data (Palisch et al., 2010). The fluid volumes ranged from 2,000 to 2,400 gallons of fresh water per gross interval using low proppant concentrations of less than 0.5 ppg. and low polymer concentrations of less than 20 lb per 1,000 gallons (Schein, 2004). One of the major disadvantages of slickwater fracturing was inefficient proppant transport and placement. Premature proppant settling would leave the top portion of the fracture unpropped. Furthermore, the low-viscosity fluid created narrower dynamic fracture widths. This is why smaller size proppant of 100, 40/70, and 30/50 mesh are used. It is likely that even the smallest proppant particles would fail to enter some of the fine fractures or places obstructed by pinch points. However, the composite effect of shear displacement, fracture roughness and uneven proppant distribution could create sets of pillars, arches, and void spaces which could enhance conductivity (Palisch et al., 2010).

1.2 Literature review

Shale fracture conductivity is the critical deliverable of hydraulic fracturing as it is directly related to well productivity. The conductivity is affected by a number of factors such as closure stress, proppant type, proppant grain size and concentration, proppant placement and distribution, non-Darcy and multiphase flow effects, temperature, gel damage, rock mechanical properties, and residual fracture width as a result of shear displacement and fracture face roughness. The distribution of hydraulic fractures, their geometry, dimensions, and contact with natural fractures are very difficult to measure or predict due to the extremely heterogeneous nature of shale formations.

Rock mechanical properties, fracture displacement, fracture roughness, and closure stress were reported in the literature to have an important effect on fracture conductivity. Bandis et al. (1983) studied the effect of rock joint deformations by taking into account factors such as normal and shear stresses, joint displacement, joint surface roughness, asperities strength and distribution, etc. Barton et al. (1985) coupled rock strength, shear displacement and normal stress with conductivity. Olsson et al. (1993) conducted series of experiments to investigate the resulting flow rates through a natural fracture of the Austin Chalk as a function of shear offset and slip. They reported that a decrease of effective normal stress on existing fractures can cause frictional sliding. The resulting shear slippage of well-matched fracture surfaces may result in significant and permanent increase in permeability due to newly created or enlarged apertures as a result of the shear displacement. Compressive stress, rock strength, fracture roughness, and

fracture shear displacement are factors with significant impact on fluid flow through fractures in various rock types (Makura et al., 2006).

Evidence of residual fracture widths was observed in field studies (Branagan et al., 1996) as well as under laboratory conditions (van Dam et al., 1998). The composite effect of shear displacement of opposing fracture faces and surface roughness results in residual fracture widths in the absence of proppant (van Dam et al., 1999). These studies support the belief that unpropped fractures may significantly contribute to overall well productivity especially if they exist in large numbers within the fracture network (Walker et al., 1998; Mayerhofer et al., 1997, 1998).

Investigators have shown that when proppant is present in the fracture, factors such as proppant concentration, size, and strength, closure stress have an impact on fracture conductivity. Cooke (1973) conducted laboratory experiments using brine and oil to study the permeability of a proppant pack squeezed between two steel sheets at varying stress levels using Brady sand of various sizes. He determined that conductivity has an inverse relationship with closure stress and later showed that gel residue can significantly reduce in-situ conductivity (Cooke, 1975). The first short-term conductivity standard procedure was documented by the American Petroleum Institute in API RP-61 (1989). Penny (1987) developed experimental procedures and equipment for long-term conductivity testing of proppants placed between two metal shims or two Ohio sandstones. The measurement conditions ranged from 3,000 psi and 150°F to 10,000 psi and 300°F and common proppant concentrations were used (2 lb/ft^2). Rivers (2012) performed conductivity measurements using Berea sandstone core samples with 16/30

high strength uncoated and resin coated ceramic proppant at very high areal concentrations ranging from 4 lb/ft^2 to 8 lb/ft^2. He determined that high closure stresses reduce fracture conductivity due to high degree of compaction of the proppant pack. He also concluded that higher proppant concentrations provide less conductivity and coated proppant performed better than uncoated proppant. Cyclic loading experiments showed that higher conductivity values at lower closure stresses cannot be regained due to permanent damage and the partially reversible process of compaction. Awoleke et al. (2012) performed dynamic conductivity measurements using a modified API conductivity cell to investigate the effect of closure stress, temperature, polymer loading, proppant concentrations and presence of breaker on fracture conductivity. They used sandstone cores with flat surfaces, 30/50 mesh ceramic proppant at concentrations of 0.5 to 2 ppg, polymer concentration of 10 to 30 pounds per 1,000 gallons, temperature up to 250°F and maximum closure stress of 6,000 psi. They concluded that high polymer loadings and absence of breaker lead to low conductivity values while low proppant concentrations yield high fracture conductivity due to the formation of channels in the proppant pack.

All the studies mentioned above were performed with parallel, flat sandstone core faces or parallel steel sheets used to confine moderate to high proppant concentrations. Fredd et al. (2001) investigated the effects of shear displacement and low proppant concentrations (0, 0.1, and 1.0 lb/ft^2) on fracture conductivity using Texas Cotton Valley fractured sandstone cores. He performed long-term conductivity measurements by using 2% KCL brine and 20/40 sintered bauxite ceramic proppant or

Jordan sand at temperature of up to 250°F and 7,000 psi closure stress. The results from the study showed that displaced fractures can provide sufficient conductivity in the absence of proppant. High-strength proppant reduces the effects the surface topography on conductivity even at concentrations of 0.1 lb/ft^2. In the absence of proppant conductivity may vary by several others of magnitude and it is dependent on the size and distribution of surface asperities.

Currently, there are many publications based on laboratory experiments with sandstone cores and large high-strength proppant particles that study how gel damage, fracture geometry and closure stress affect fracture conductivity. However, there are not a sufficient number of publications in the literature that discuss the effect of proppant distribution, concentrations or size on fracture conductivity. This study examines the results from experimental studies using real naturally or artificially fractured shale core samples.

1.3 Problem description

The large number of massive hydraulic fracturing operations in the United States has increased the demand for proppant in the past several years. Proppant transportation, scheduling, and storage are associated with high costs due to increasing competition among operating companies involved in oil and gas production from organic-rich shale reservoirs. One way to improve well economics is to optimize the hydraulic fracturing design by reducing the cost of the treatment. Fracture conductivity, defined as the product of fracture permeability and fracture width, is a key parameter which determines

well productivity and ultimate recovery from ultra-low permeability formations. From a design standpoint, the controllable factors that affect conductivity are proppant strength, proppant size and concentration, fracturing fluid viscosity, treating pressure and pumping flow rate. During the slickwater fracturing era in the Barnett shale the use of low viscosity fluid and low proppant concentrations enhanced fracture conductivity and significantly improved well economics regardless of narrower fractures with less proppant layers inside, poor vertical proppant placement, and unevenly distributed stress concentrations on individual grains in the case of pillars, arches, and void spaces (Palisch et al., 2010) or in the case of a proppant partial monolayer (Brannon et al., 2004).

This study presents the results from a series of laboratory conductivity measurements using real Barnett shale core samples with natural and induced fractures. The induced fractures were configured to be either aligned or displaced to simulate the effect of shear displacement on fracture conductivity which is evident from microseismic studies (Warpinski et al., 2012). The effect of various proppant sizes at different concentrations was also investigated including a case of a partial monolayer.

1.4 Research objectives

The conductivity of fractures in highly heterogeneous shale formations can be accurately determined by conducting laboratory experiments. This research had the following objectives:

1. Set up an experimental procedure that allowed consistent static laboratory conductivity measurements using real Barnett shale core samples. The samples were loaded in a modified API conductivity cell.
2. Measure the conductivity of propped and unpropped natural and induced fractures by taking into account fracture roughness and the presence of naturally occurring cementing material.
3. Study the effect of shear displacement on fracture conductivity in the presence or absence of proppant
4. Investigate the effect of proppant size and concentration on fracture conductivity.

By achieving these objectives, this work is able to shed more light on fracture conductivity in shale reservoirs by presenting the results from 61 successful experiments. This study also established a well-tested procedure and workflow for future laboratory work using core samples from different shale formations.

2. LABORATORY APPARATUS AND EXPERIMENTAL PROCEDURE

2.1 Description of laboratory apparatus

The American Petroleum Institute (API) developed a standard for short-term laboratory conductivity measurements to unify experimental design and procedures in different laboratories and provide repetitive and reliable results for comparison. The experimental equipment and procedures were documented in API RP-61. The fracture conductivity setup allowed for pumping real fracture fluid with cross-linkers and breakers through a proppant pack confined between two sandstone cores. The setup could simulate field conditions of proppant performance. The proppant was placed manually. The conductivity was calculated by measuring the flow rate and pressure drop across the core length at various closure stresses.

This study used a modified American Petroleum Institute (API) conductivity cell to perform short-term static fracture conductivity measurements at room temperature by flowing dry nitrogen gas through natural and induced fractures of Barnett shale using white sand of various sizes and concentrations as proppant. **Fig. 1** shows a schematic of the experimental setup up. The fracture conductivity laboratory apparatus consists of the following components:

- Nitrogen tank
- Gas flow controller
- CT-250 hydraulic load frame
- Modified API conductivity cell

- Three pressure transducers
- Needle valve as a back pressure regulator
- Flow lines
- Data acquisition system

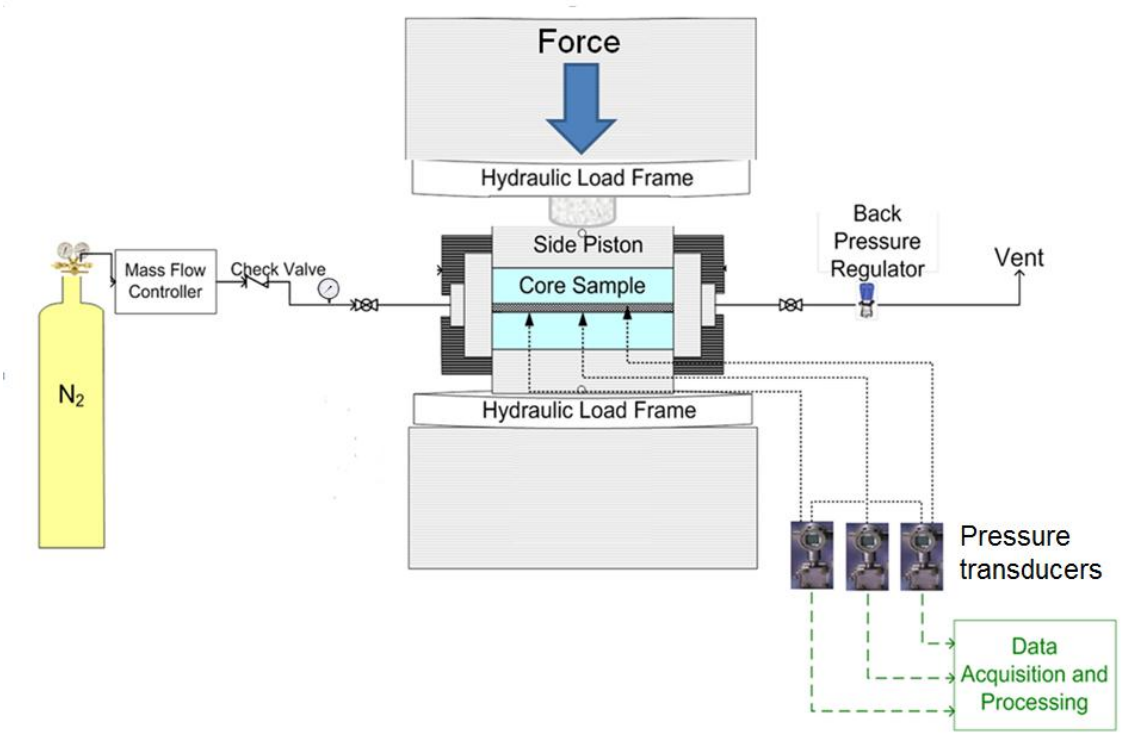

Fig. 1 – Schematic of fracture conductivity laboratory setup

The nitrogen tank is pressurized up to 2,000 psi and is controlled by a very sensitive spring valve. The mass flow controller is capable of measuring a maximum

flow rate of 10 standard liters per minute with an accuracy of 0.001 standard liter per minute.

The load frame is capable of applying up to 870 kN force or around 16,000 psi of closure stress on a piston with surface area of 12 in^2. It can apply closure stress at a rate of 100 psi per minute. The piston's axial displacement is recorded with an accuracy of 0.01 millimeters.

The modified API conductivity cell is made of stainless steel and consists of a cell body, two side pistons and two flow inserts (**Fig. 2**). The cell body is 10 in. long, 3-1/4 in. wide, and 8 in. in height. The hollow section of the cell is designed to accommodate a pair of core samples that are 7 in. long, 1.65 in. wide, and 3 in. in height. The top and bottom pistons keep the cores in place and have Viton polypack seal to prevent any fluid leakage. Each piston is 7 in long, 1.65 in. wide, and 3 in. tall and has a hole drilled into its center that is connected to leak-off lines and serves as a conduit of fluids out of the cell during an experiment. The two flow inserts with Viton o-rings connect to flow lines on the upstream and downstream side of the cell.

There are three pressure measuring ports drilled through the middle of one side of the cell body. Two of the transducers are used to measure the differential pressure across the length of the fracture while the third one in the middle of the cell is measuring the absolute cell pressure. The transducers can measure the pressure with an accuracy of 0.01 psi. The needle valve connected on the downstream side of the system serves as a back pressure regulator which is used to control the flow rate during the conductivity measurements.

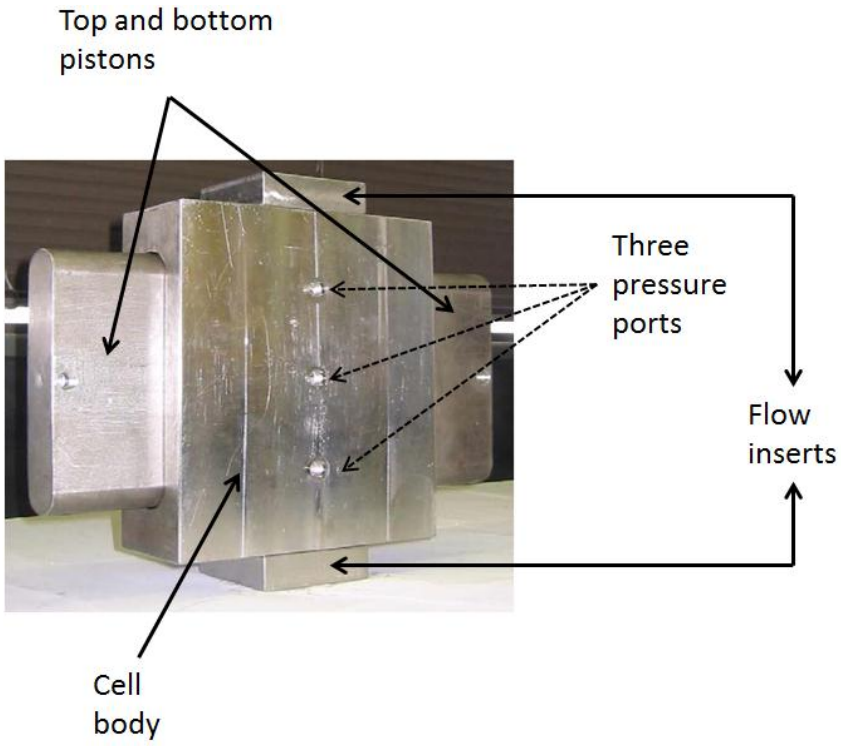

Fig. 2 – Modified API conductivity cell

2.2 Experimental procedure

Figure 3 shows a schematic of the three major steps of the experimental procedure:

Fig. 3 – Experimental steps for fracture conductivity measurements

2.2.1 Barnett shale overview

The Barnet shale is of Mississippian age and is situated in the Fort Worth Basin of north-central Texas. The shale is a very heterogeneous, naturally fractured reservoir characterized with very low matrix permeability in the micro- to nano-Darcy range (0.00007 to 0.005 md) and low porosity in the 4-6% range (Coulter et al., 2004). The natural fractures occur in clusters and have limited vertical extent. The formation consists of 1/3 quartz, 1/3 clays, and 1/3 other minerals including 10% carbonates, 12% kerogen. The average total organic content is about 4.5% (Lancaster et al., 1992).

This experimental work was designed to study the fracture conductivity in shale formations and therefore, Barnett shale samples with preserved natural fractures were cut out of shale blocks collected from a quarry in San Saba, Texas. **Fig. 4** shows a picture of a typical shale block from the outcrop (right) and the complexity of the fracture network in this shale formation (left).

Papazis, (2005) identified five main types of lithology in the Barnett shale based on analysis of cores and outcrops: black to greyish shale, calcite-rich mudstone or limestone, silt-rich black shale, coarse grain accumulations, concretions. The shale core samples used in this work were identified as black to greyish shale as shown on **Fig. 5**. This type of shale is usually associated with natural fractures filled with calcite that can remain open (Papazis, 2005).

Fig. 4 – Barnett shale outcrop and fracture complexity

2.2.2 Core sample preparation (Barnett shale)

The shale samples were cut into dimensions suitable for the modified API conductivity cell. Because it was extremely difficult to identify and cut whole 3 in. thick shale cores due to the very brittle nature of the highly laminated shale blocks and the presence of natural fractures. It was decided that the core samples used for testing will consist of sandstone and shale. Sandstone cores made up the total thickness of 3 in. with thickness of the 1.5 – 2 in. **Fig. 5** shows the exact dimensions of the samples and a typical configuration.

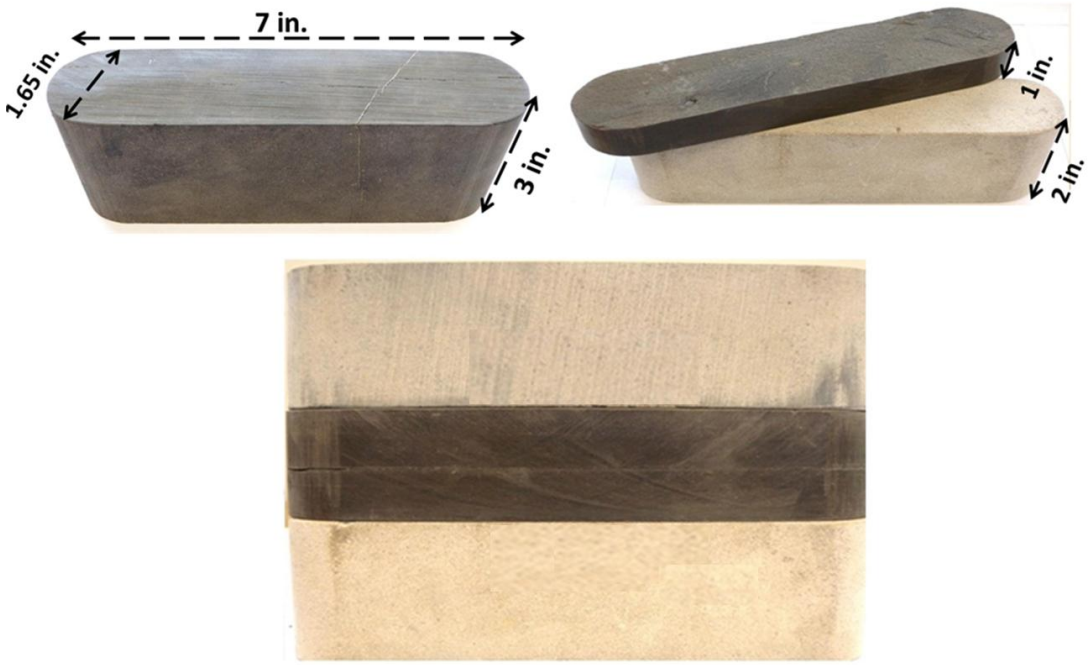

Fig. 5 – Core samples configuration and dimensions

Laboratory fracture conductivity measurements usually use core plugs with 1 or 1.5 in. in diameter. However, these measurements are limited in scale and cannot account for the effect of fracture roughness and particle mobility (Morales et al., 2011; Ramurthy et al., 2011). The shale cores used in this study were shaped to fit the modified API conductivity cell. They were fractured carefully along the laminated bedding plane. The cores that contain natural fractures were treated carefully to preserve the loosely attached infill material. It was important to keep the vibrations to a minimum while cutting the sample and to avoid tilting or shaking it during transportation. Finally, different types of fractured were identified from the available samples and the experimental study began.

The Barnett shale core samples were coated with a silicone-base sealant using a mold to perfectly fit into the conductivity cell. The previous coating procedure was prepared to coat each core sample separately since the mold was design for 3-in thick core samples with flat surfaces. Since the shale samples have irregular surfaces, the procedure was modified to make sure that the fracture is fully sealed especially during the conductivity measurements in the absence of proppant. Using the modified procedure, the coating of the core samples was done in three stages.

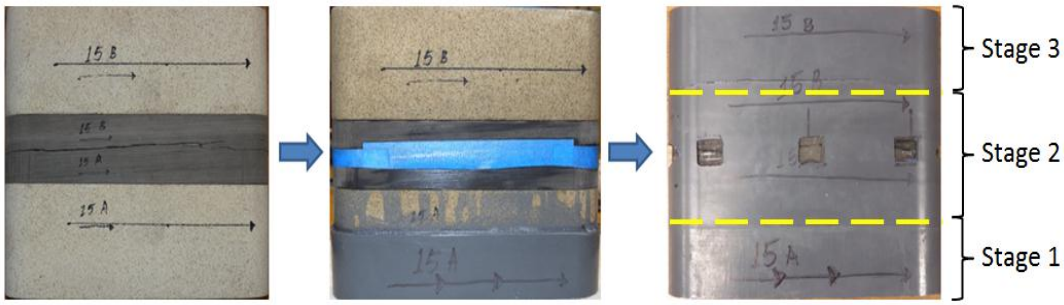

Fig. 6 - Core sample preparation procedure

Fig. 6 illustrates the basic steps of the procedure. The first stage involved the coating only of 1.5 – 2 in. of the bottom sandstone core. The second stage was designed to coat 3 in. of the middle section which contained the fracture. Finally, the third stage coated the remaining 1.5-2 in. of the top core sample. The detailed preparation procedure for a single stage is outlined below:

1. Glue the shale core to the sandstone core using Gorilla glue to create a single 3-in. thick sample. *Follow the gluing instructions provided by the Gorilla glue manufacturer.*
2. Carefully remove the glue sticking outside the glued area using a razor blade and sand paper.
3. Disassemble the aluminum mold used for coating the core samples as shown on **Fig. 7.**

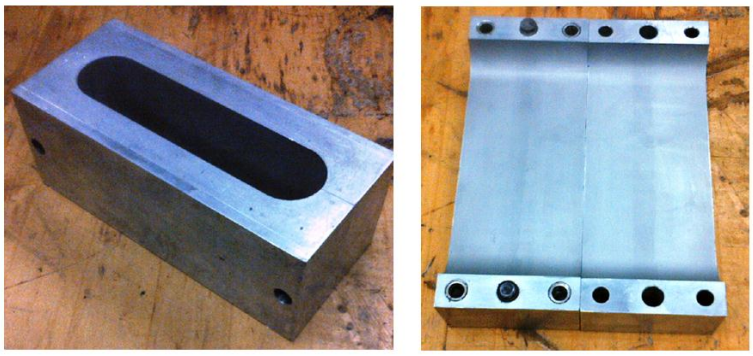

Fig. 7 – Aluminum mold used for core sample coating

4. Carefully clean the mold inner surface with acetone using paper towel or soft cloth. *Do not use any sand paper or metal tools to avoid any damage to the surface which must remain perfectly smooth.*
5. Label the rock samples with a permanent marker
6. Apply silicon primer with a brush on the outer surface of the core sample. Apply the primer three times and wait 10-15 minutes between each application.

7. Spray silicon mold release agent on the cleaned inner mold surfaces. Repeat three times. Wait for 3-5 minutes between each application.
8. First stage only: wrap three layers of Teflon tape around the top of an already coated sample and insert it into the mold covering 1-1.5 in. of the height of the mold.
9. First stage only: Assemble the mold around the inserted core and tighten the bolts. The Teflon tape should provide a good seal and prevent any leakage. Use two metal or wooden blocks of 1-1.2 inch thick to provide support for the mold.
10. First stage only: Place the core into the mold (only 1.5-2 inches of the sandstone block should be inside the mold.
11. Second stage only: Apply 3M blue painters or white masking tape around the fracture to prevent encroachment of the epoxy while it is in liquid state.
12. Second stage only: wrap three layers of Teflon tape around the top of the first stage coating to prevent any leakage once the mold is assembled to cover the middle part of the core setup. Use two metal or wooden 1-1.2 in. thick blocks to provide support for the mold.
13. Third stage only: wrap three layers of Teflon tape around the top of the second stage coating to prevent any leakage once the mold is assembled to cover the middle part of the core setup. Use two metal or wooden 3-4.5 in. thick blocks to provide support for the mold.
14. Prepare 50 grams of silicon potting compound and 50 grams of silicon curing agent from the RTV 627 kit. Make sure that the mixing ration is 1:1 either by

volume or weight percent. Mix the fluid well. Avoid contaminating it with small particles or debris. Let it sit for 30-40 minutes to let all trapped air bubbles to come out. This step is critical for successful sample coating.

15. Pour the potting compound mixture very slowly and carefully. It is recommended to pour the fluid from one side of the mold to prevent air from being trapped between the mold inner surface and the core sample. Once you have poured half of the fluid, wait for 1-2 minutes to allow the viscous mixture to settle down and let any trapped air to come out. Continue until the entire core surface inside the mold is covered with the epoxy.
16. Let the mold sit for one hour. Check for leaks by observing the fluid level. Then let it sit for another 2-3 hours at room temperature.
17. Place the mold in the laboratory oven and leave it there for three hours at 160°F.
18. Take the mold out of the oven and let it cool down for 1-2 hours
19. Disassemble the mold. Unscrew the bolts and use a c-clamp or a hydraulic jack to remove the core sample.
20. Cut any extra silicon edges with a razor cutter.
21. Label the sample and draw an arrow indicating the direction of flow.
22. Use a razor blade to cut three windows for the pressure ports and two windows as an inlet and outlet for the flow inserts as shown on **Fig. 6**.
23. Unpropped fracture case: the core is ready to use

24. Propped fracture case: use a razor blade to carefully separate the two core samples by cutting the rubber along the middle of the sample so proppant can be placed if desired. The separated cores are ready to use.

2.2.3 Proppant placement

The proppant was manually placed and evenly distributed on the fracture face. **Fig. 8** shows an example of the distribution of 100-mesh white sand at 0.01 lb/ft^2 (right) and 0.03 lb/ft^2(left) areal concentrations.

Fig. 8—Placement of 100-mesh sand on rough fracture surface at 0.10 lb/ft^2 (right) and 0.03 lb/ft^2 (left)

1. Prepare the core sample using the detailed procedure described in section 2.2.1.
2. Wrap two rows of three layers of Teflon tape around each of the separated core samples to prevent fluid leakage in the vertical direction
3. Use an electronic scale to measure the desired amount of proppant
4. Carefully place and evenly distribute the proppant on the fracture surface of the bottom core.
5. Close the fracture by placing the second core on top and carefully aligned the two samples using the cut windows for the pressure ports as guidance.

6. Wrap two rows of three layers of Teflon tape perpendicular to the fracture length and in between the pressure port windows. This will prevent any gas migration or leakage in the horizontal direction.
7. Apply high-pressure vacuum grease around each row of Teflon tape to provide a good seal and prevent nitrogen gas leakage through microscopic gaps between the sample and the cell inner surface. The grease also facilitates the core placement into the conductivity cell without damaging the silicon coating. **Fig. 9** shows an example of a fully prepared core.

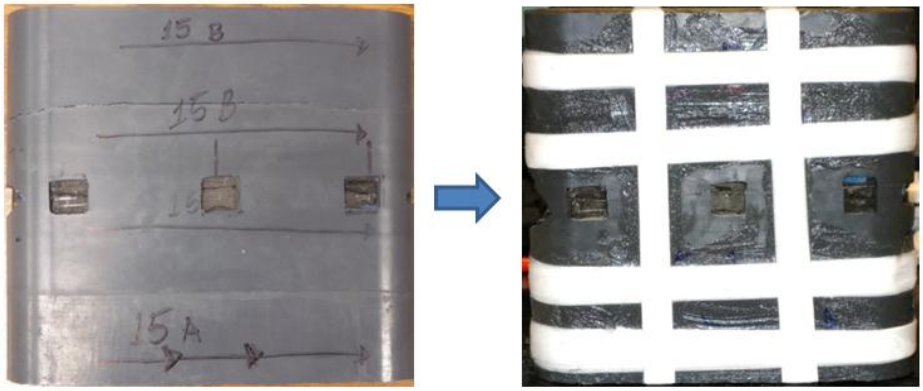

Fig. 9 – Application of Teflon tape around the core sample

8. Safely place the wrapped core into the conductivity cell using a hydraulic jack
9. Align the fracture with the flow and pressure ports of the cell
10. Place the bottom piston by lifting the cell carefully and placing it on top of the piston. Do not tilt or shake the cell to avoid proppant rearrangements in the

fracture. *All piston rubber seals must be coated with high-temperature o-ring grease to provide a good seal and prevent tear and wear.*

11. Plug the leak-off port of the bottom piston. *Wrap 2-3 layers of Teflon tape around the threaded section of the plugs to provide better seal.*
12. Place the top piston, center the cell in the load frame and apply 500 psi closure stress at increments of 100 psi per minute to stabilize the system.
13. Plug the leak-off port of the top piston
14. Mount the flow inserts.
15. Connect the flow lines and the pressure transducers. *Make sure all connections are tight*
16. The setup is ready for conductivity measurements. **Fig. 10** and **Fig. 11** show a picture of the fully assembled conductivity setup**.**

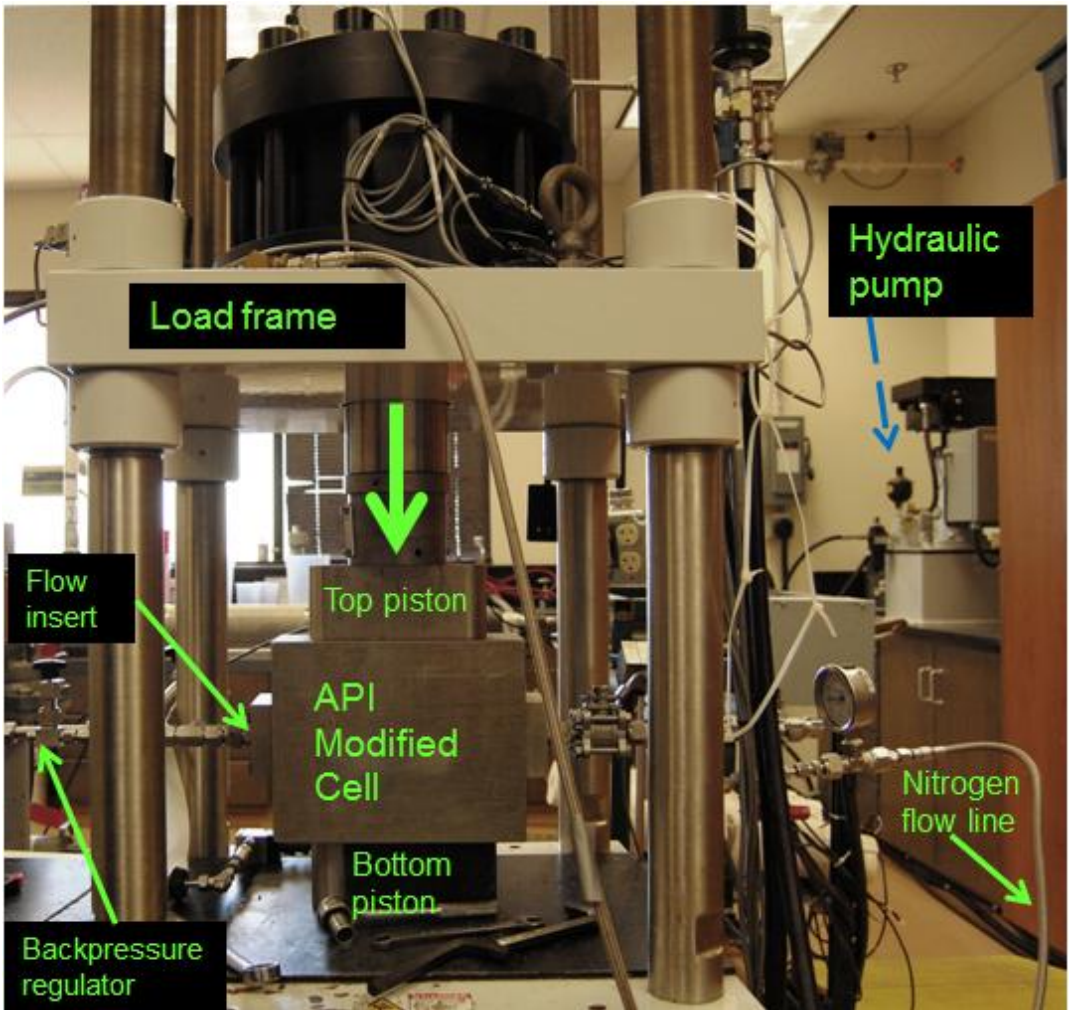

Fig. 10 – Fully-assembled laboratory apparatus (view A)

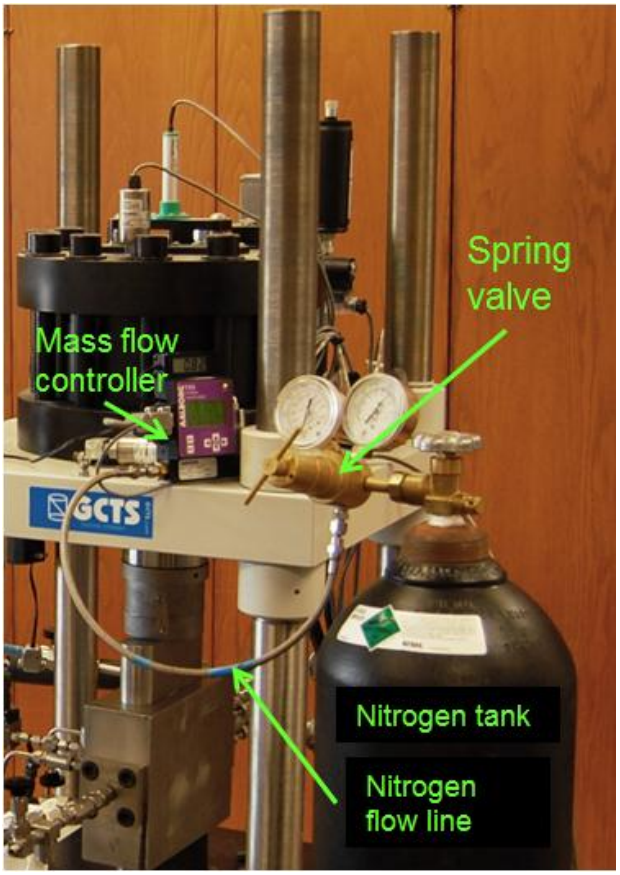

Fig. 11 – Fully-assembled laboratory apparatus (view B)

2.2.4 Fracture conductivity measurement

This experimental work involved short-term fracture conductivity measurements. Dry nitrogen gas was used to simulate gas production from fractures in the Barnett shale. The conductivity was measured at room temperature by recording the flow rate and associated pressure drop in the fracture at closure stresses of up to 4,000 psi. The conductivity was calculated using Darcy's law based on four data points recorded at each closure stress. The detailed procedure to measure conductivity is as follows:

1. Carefully follow the procedure mention in section 2.2.2. The cell is at 500 psi closure stress.
2. Turn on the mass flow controller and wait until the displayed flow rate stabilizes.
3. Record the baseline flow rate (0.25 – 0.31 standard liters per minute).
4. Close the back pressure regulator located on the downstream side of the conductivity apparatus.
5. Open the nitrogen tank.
6. Using the spring valve carefully start flowing nitrogen into the cell until the cell pressure reaches 50-55 psi and wait until it stabilizes. *Gradually increase the flow rate to up to 1.5-2 standard liter per minute to avoid movement and rearrangement of the proppants inside the fracture especially at lower closure stresses.*
7. Perform a pressure test. Check the flow rate and make sure that it is close to the baseline flow rate and not above 0.35 liters per minute. *Higher flow rates indicate gas leakage in the system and the experiment must be stopped. Begin the measurements only if the system passes the pressure test.*
8. Carefully open the back pressure regulator and adjust the desired flow rate while maintaining the cell pressure constant and close to its baseline value of 50-55 psi.
9. Wait until a stable gas flow through the fracture is established (i.e. when the flow rate and the differential pressure are constant). *It is recommended to not exceed a flow rate of 1.0 liters per minute to avoid turbulent flow and non-Darcy flow effects).*

10. Record the flow rate, cell pressure, pressure drop and export the data. *For measurement accuracy, the differential pressure must not exceed 10% of the cell pressure. This is because gas is highly compressible.*
11. Repeat steps 6 through 9 four times to take four measurements at a given closure stress. This ensures the consistency and accuracy of the measurement from a statistical standpoint.
12. Increase the closure stress to the next desired level at a rate of 100 psi per minute and leave the back pressure regulator slightly open to prevent any excessive gas pressure build up in the fracture during the process.
13. Once the desired closure stress is reached, wait for 30 minutes until the system is stable and there is no change in the axial displacement of the load frame piston.
14. Once the system becomes stable, close the back pressure regulator and adjust the cell pressure to its baseline pressure using the spring valve attached to the nitrogen tank.
15. Repeat steps 6 to 11 as many times as needed depending on the experimental design. *It is recommended to use similar flow rates during the measurements at each closure stress.*
16. Once the experiment is finished, close the nitrogen cylinder valve and the spring valve.
17. Open the back pressure regulator to bleed off the trapped pressure inside the cell. *Do not fully open the back pressure regulator if that would result in differential*

pressure, higher than the maximum pressure rating of the diaphragm in the pressure transducer.

18. Disconnect all flow lines and pressure transducers, remove the flow inserts and the top piston's plug while the system is stable and closure stress is applied.
19. Gradually lower the closure stress and lift the load frame piston.
20. Remove the top piston of the cell.
21. Secure the cell and remove the plug from the leak-off port of the bottom piston.
22. Use the hydraulic frame to carefully remove the bottom piston and the core sample.
23. Shut down the load frame hydraulic pump.
24. Switch off the data acquisitioning system.
25. Bleed off the trapped pressure in the spring valve: *Make sure the nitrogen tank valve and the spring valve are closed; disconnect the flow line; slowly open the spring valve until the gas comes out.*
26. Unplug the flow rate controller adapter from electrical outlet.
27. Clean the cell.

2.2.5 Fracture conductivity calculation

The conductivity of the fracture at each closure stress was calculated based on the four measurements of cell pressure (P_{cell}), flow rate (q), and differential pressure (Δp) using Darcy's law (Eq. 1.1).

$$-\frac{dp}{dL} = \frac{\mu v}{k} \quad \text{.....} \quad (1.1)$$

The gas flux is $\frac{W}{A} = \rho v$ and according to the real gas law $\rho = \frac{pM}{zRT}$. The two sides of Eq. 1.1 are multiplied by ρ:

$$\rho\left(-\frac{dp}{dL}\right) = \rho\frac{\mu v}{k} \quad \text{(1.2)}$$

Applying the real gas law:

$$-\frac{M}{zRT}pdp = \frac{W\mu}{Ak}dL \quad \text{(1.3)}$$

Integrating Eq. 1.3 yields:

$$\frac{M}{zRT}\frac{(p_1^2 - p_2^2)}{2} = \frac{W\mu L}{Ak} \quad \text{(1.4)}$$

The gas velocity in the fracture equals $\frac{q}{w_f h_f}$ and therefore,

$$\frac{M(p_1^2 - p_2^2)}{2zRTL} = \frac{\rho\mu q}{h_f}\frac{1}{k_f w_f} \quad \text{(1.5)}$$

By plotting $\frac{M(p_1^2 - p_2^2)}{2zRTL}$ on the y-axis and $\frac{\rho\mu q}{h_f}$ on the x-axis, the slope of the line is the inverse of fracture conductivity, $k_f w_f$ where k_f is the fracture permeability and w_f is the fracture width after closure. **Table 1** shows the parameters used to calculate conductivity.

Table 1 – Fracture conductivity calculation parameters.

Pressure drop Length	L_f	5.25	in.
Fracture face width	h_f	1.65	in.
Molecular mass of nitrogen	M	0.028	kg/mole
Compressibility factor	z	1.00	
Universal gas constant	R	8.3144	J/mol-K
Temperature	T	293.15	K
Viscosity of nitrogen	μ	1.7592E-05	Pa.s
Density of nitrogen	ρ	1.16085	kg/m3
Atmospheric pressure	P_{sc}	14.7	psi
Differential pressure (measured)	Δp	variable	psi
Flow rate (measured)	q	variable	liter/min

2.3 Experimental design matrix and conditions

Barnett shale wells were fractured with "slickwater" treatments that consisted of pumping low viscosity fluid carrying low proppant concentrations ranging from 0.25 to 1.0 pounds per gallon of fluid (Palisch, 2010). Proppant size of 100-mesh, 40/70-mesh are commonly used during slickwater fracturing operations. Larger grain sizes of 30/50 or 20/40-mesh are pumped primarily during the tail-in stages to ensure high near-wellbore fracture conductivity (Coulter, 2004). Slickwater fracturing creates very complex fracture networks in the Barnett shale which is evident from microseismic data (Palisch et al., 2010). Shear slippage between the fracture walls was also reported in the literature (Warpinski et al., 2012). Therefore, it is very likely that there are a great number of displaced fractures that do not completely match after closure. The resulting residual fracture widths may contribute to fracture conductivity and well productivity. Furthermore, the poor proppant placement efficiency of the low viscosity fluid suggests

that the proppant distribution and areal concentration in the fractures can be highly variable, if any proppant is present at all. **Fig. 12** shows a schematic of a fracture where the proppant settled in the bottom of the fracture leaving the top unpropped with some residual fracture width (Britt et al., 2006). The fracture width is usually reduced towards the tip. Small fracture widths mean fewer proppant layers which would greatly increase the average stress concentration on each proppant grain (Palisch et al., 2010).

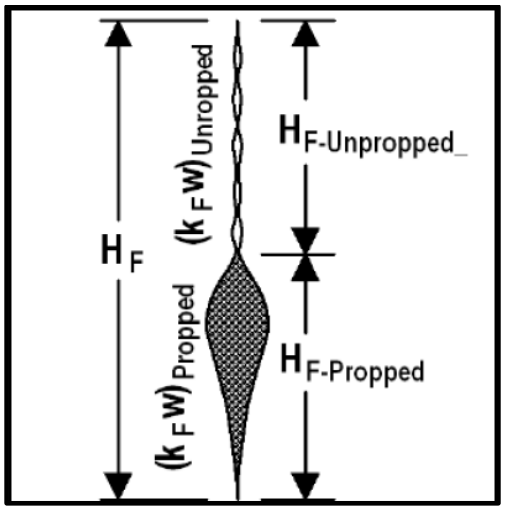

Figure 12 - Schematic of a half propped fracture as a result of proppant settling (Britt et al., 2006)

In this experimental study, four main fracture types were identified and their conductivity was measured in the absence of proppant and using 100-mesh, 40/70-mesh and 30/50-mesh white sand placed at areal concentrations from 0.03 to 0.20 lb/ft^2. Displaced fractures with no proppant or with low proppant concentrations were studied

because they represent more closely the realistic conditions in the fracture network. **Fig. 13** shows the experimental design matrix.

Fracture Type		Proppant Concentration [lb/ft²]	Proppant Mesh Size
Natural fractures	Well-cemented	unpropped	100
	Poorly-cemented	0.03	40/70
Induced fractures	Aligned	0.06	30/50
	Displaced	0.1	
		0.2	

Fig. 13 –Experimental design matrix

2.3.1 Natural fractures (Barnett shale)

The collected shale blocks from the Barnett shale outcrop were highly fractured. Many core samples used in this study were cut with preserved natural fractures. The fractures were filled with cement which was determined to be anhydrite. **Fig. 14** shows the results from the Scanning Electron Microscope-Energy Dispersive X-ray tests.

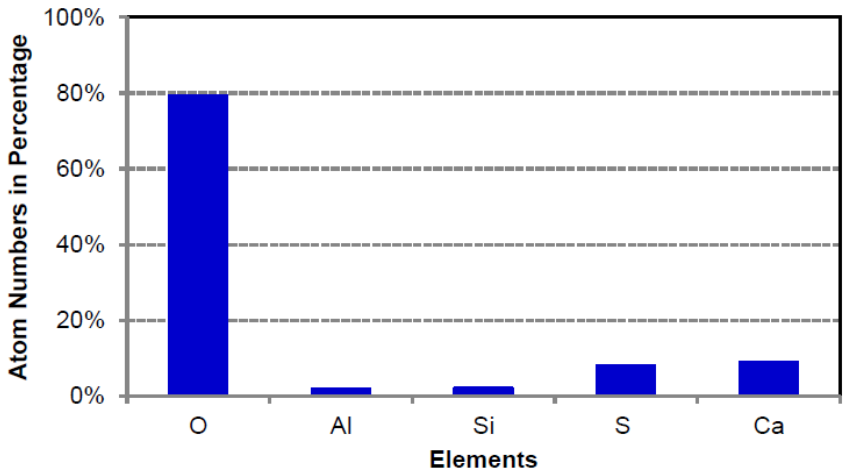

Fig. 14 – Atomic composition of fracture infill material

Oxygen, calcium and sulfur were the dominant elements that comprise the fracture infill material. Based on the condition and amount of cement present in the fracture, two main natural fracture types were identified: (1) well-cemented fractures and (2) poorly-cemented fractures. **Fig. 15** shows an example of a well-cemented fracture. This type of fracture was glued by the cement which acts like proppant since it keeps the fracture open.

Fig. 15 – Well-cemented natural fracture

The poorly-cemented fracture faces were not glued and the cementing material was loosely attached to the fracture surface. It is likely that some of the infill material was lost during handling, transportation or cutting. Therefore, those fractures were split into two categories based on the amount of cementing material: (1) fully-filled and (2) partially-filled. **Fig. 16** shows an example of the two poorly-cemented fracture types.

The conductivity of the natural fractures was studied to gain better understanding of how the irregular fracture faces and the fracture infill deposits affect fracture conductivity with and without proppant.

Fig. 16 – Fully-filled (top) and partially-filled (bottom) poorly-cemented natural fractures

2.3.2 Induced fractures (Barnett shale)

The shale cores that did not contain natural fractures were artificially fractured along the laminated bedding planes to create fractures with rough surfaces. A set of fractured samples were offset by 0.1 in. and then cut to represent displaced fractures with non-matching surfaces as a result of shear displacement. The induced fractures were divided into two categories: (1) aligned and (2) displaced. **Fig. 17** shows a schematic of propped and unpropped induced fractures.

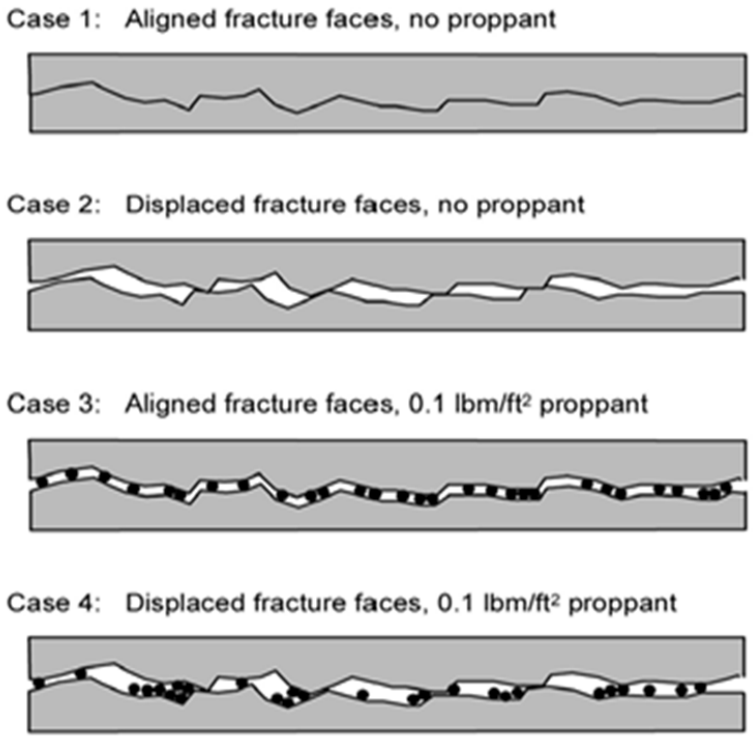

Fig. 17 – Possible fracture configurations as a result of slickwater fracturing (Fredd et al., 2001)

The conductivity of these new shale fracture configurations with preserved surface topography was measured to investigate the effect of residual fracture width in combination with low proppant concentrations on shale fracture conductivity.

2.3.3 Proppant size and concentration

One of the goals of this experimental study was to investigate the effect of various sizes at low concentrations in induced and natural fractures with non-matching rough surfaces. The fracture conductivity was measured using 100-mesh, 40/70-mesh and 30/50-mesh white sand that was widely used in slickwater fracturing treatments in the Barnett shale. The sand was manually placed on the shale surfaces at concentrations of 0.03 lb/ft^2, 0.06 lb/ft^2, 0.10 lb/ft^2 amd 0.20 lb/ft^2. These concentrations are roughly equivalent to 0.25 ppg, 0.50 ppg, 0.75 ppg, and 1.50 ppg. that are commonly used in slickwater fracturing assuming a dynamic fracture width of 0.2 in.

2.3.4 Sieve analysis

The proppant used in this work was natural white sand of three different sizes: 100-mesh, 40/70-mesh and 30/50-mesh. The sand used for each laboratory experiment was sampled from a 5-gallon bucket. Sieve analysis was performed to understand the grain size distribution of each sand size. The results are shown in **Figs. 18 through 20.** Most of the 100-mesh sand (47.2%) was retained in the 100-mesh sieve. The rest of the grains were contained in the 70-mesh, 140-mesh and 170-mesh sieves (16.7%, 22.5% and 4.3% respectively). Only a small portion of the 40/70-mesh sand was retained in the 40-mesh sieve. About 95% of the 40/70-mesh sand particles were retained in the 50-

mesh and 70-mesh sieves (49% and 46% respectively). The bulk part of the 30/50-mesh sand particles were retained in the 40-mesh and 50-mesh sieves (35% and 60% respectively).

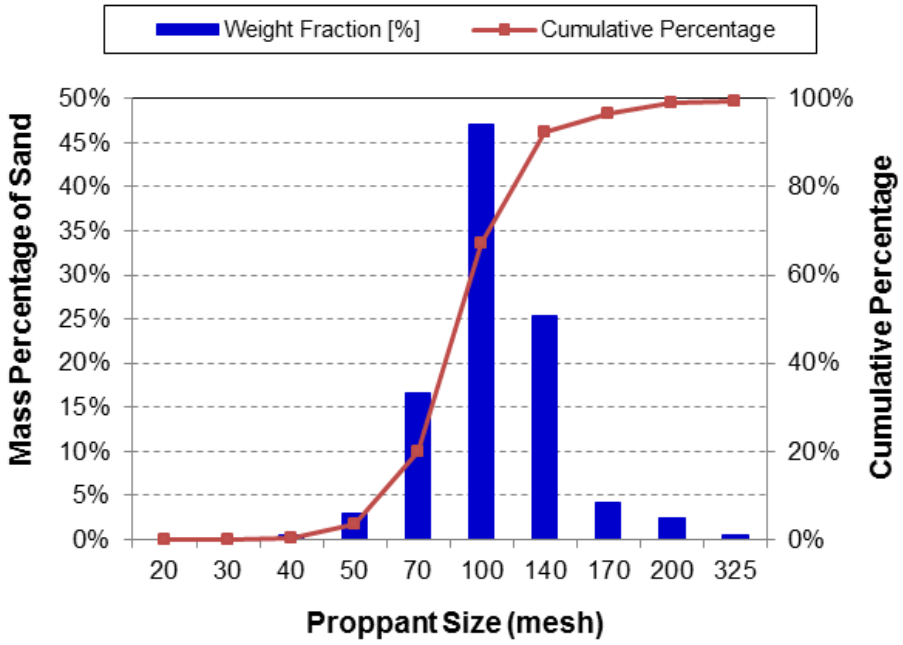

Fig. 18 – Grain size distribution of 100-mesh white sand

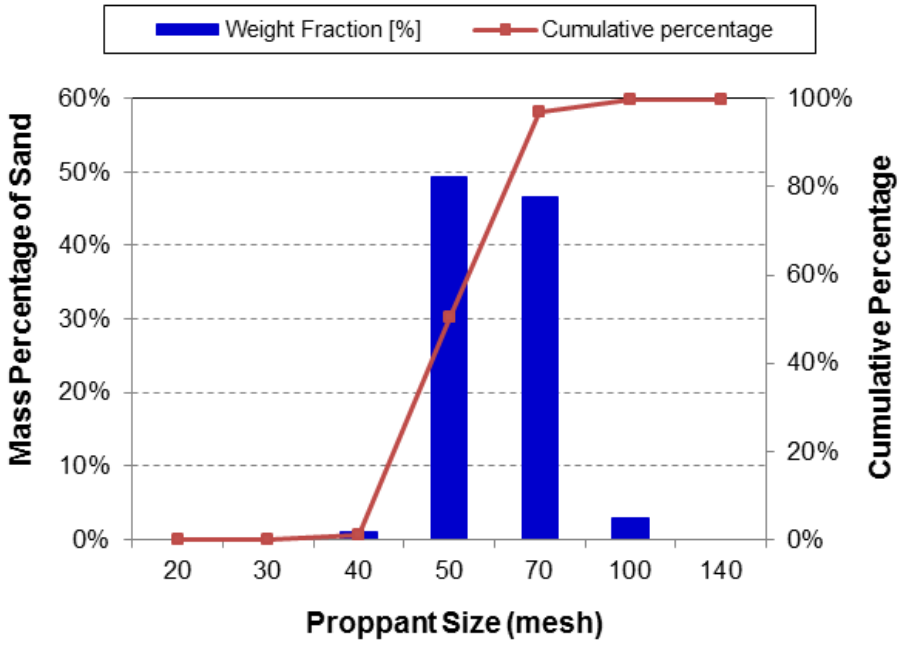

Fig. 19 – Grain size distribution of 40/70-mesh white sand

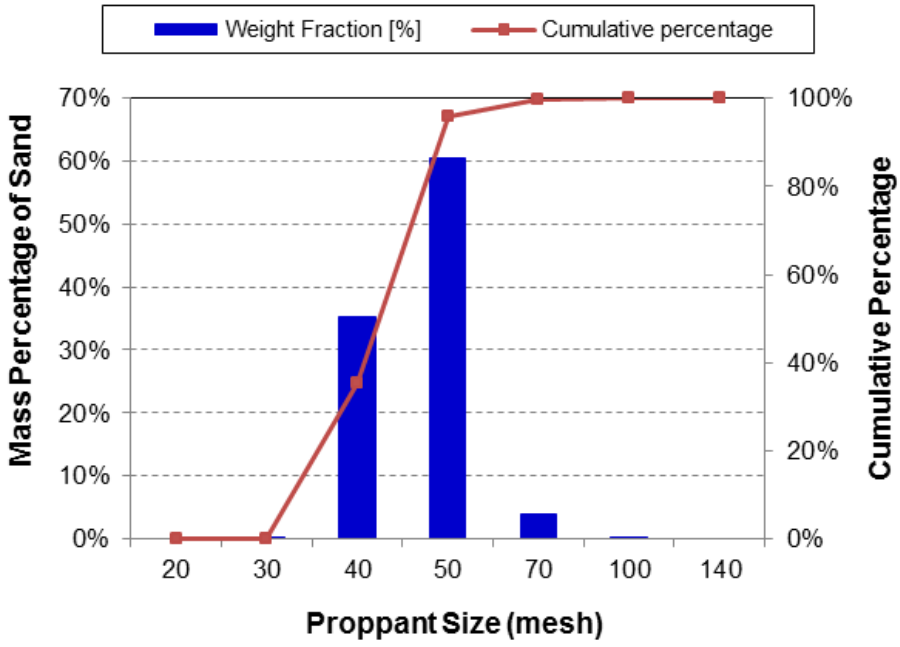

Figure 20 – Grain size distribution of 30/50-mesh white sand

2.3.5 Proppant partial monolayer

Darin and Huit (1960) showed that ultra-low areal proppant concentration and the resulting partial monolayer has void spaces and channels that can provide a better conductive path than a full monolayer or proppant packs with a few layers. **Fig. 21** shows an illustration of a partial monolayer. Many field trials to create a monolayer with natural sand and slickwater fracturing failed due to the poor proppant transportation properties of the low viscosity fracturing fluid. Fracture width can also be reduced due to insufficient proppant strength or embedment in the case of a monolayer.

This experimental work studied the effect of a partial monolayer on fracture conductivity. The 30/50-mesh and 40/70-mesh sand formed partial monolayers at ultra-low areal concentrations of 0.03 lb/ft^2 and 0.06 lb/ft^2 (30/50-mesh only). The larger grains resulted in smaller number of grains per unit weight. A special case using grains with more uniform size distribution (retained in the 40-mesh sieve) was designed to compare the partial monolayer and proppant pack performance at concentrations of 0.03 lb/ft^2 and 0.20 lb/ft^2.

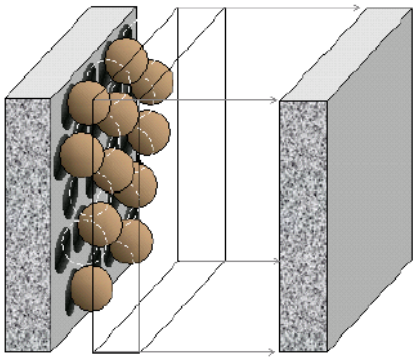

Fig. 21 – Schematic of proppant partial monolayer (Brannon, 2004)

3. EXPERIMENTAL RESULTS AND DISCUSSION

A series of fracture conductivity experiments was performed using Barnett shale cores with different types of fractures. Some of the core samples were used in multiple conductivity experiments for consistency. Unpropped fracture conductivity was used as an indicator of any damage to the shale fracture surface. The unpropped conductivity was measured after each set of experiments. It usually remained unchanged which means that the fracture surface asperities were not significantly deformed or altered during previous experiments. **Figs. 22 and 23** show examples of fracture conductivity of aligned and displaced unpropped fracture before and after a propped fracture experiment.

Tables 2 through 4 show a summary of the experimental work for natural well-cemented and poorly-cemented fractures and induced fractures with aligned and displaced fracture faces. The conductivity of unpropped fractures depends on several important factors:

1. rock mechanical properties
2. infill material properties
3. degree of fracture surface roughness
4. shear displacement
5. residual fracture width
6. aperture size distribution in the fracture
7. degree of aperture connectivity
8. number and distribution of contact points

Propped fracture conductivity depends on proppant strength, size, concentration, degree of compaction, rearrangement, embedment etc. All these factors are interrelated and difficult to measure individually. In this study, variations of measured fracture conductivity under different conditions were indicative of the effect of some of the factors mentioned above.

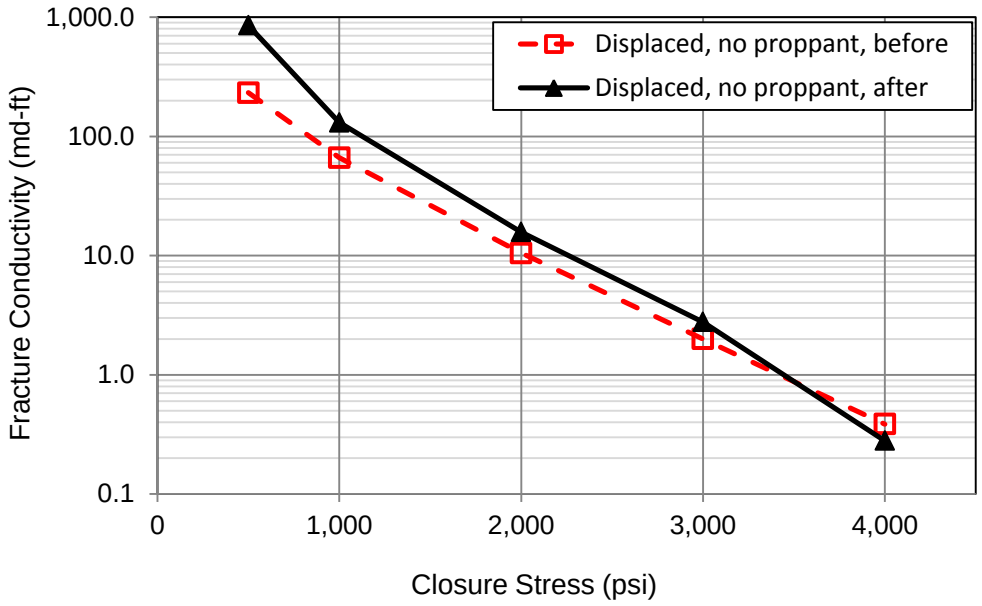

Fig. 22 – Conductivity of a displaced unpropped fracture before and after a propped fracture conductivity measurement

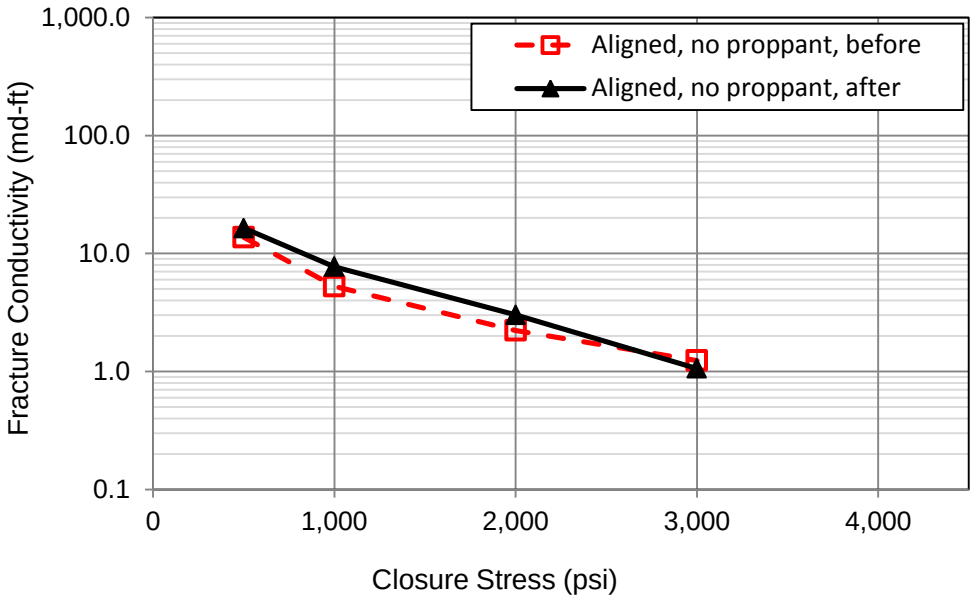

Fig. 23 – Conductivity of aligned unpropped fracture before and after propped fracture conductivity measurement

Table 2—Experimental design matrix: natural fractures.

Fracture Type	Natural Fracture									
Fracture Infill	Well-cemented		Poorly-cemented							
Proppant size (mesh)	No Prop.	100	No Prop.	No Prop.	No Prop.	No Prop.	100	100	40/70	40/70
Fracture Condition	cement in place	No cement	Fully-filled, cement in place	Fully-filled, cement removed	Partially-filled, cement in place	Partially-filled, cement removed	Fully-filled, cement removed	Partially-filled, cement removed	Partially-filled, cement removed	Fully-filled, cement removed
Proppant loading (lbm/ft^2)	0	0.06	0	0	0	0	0.06	0.06	0.06	0.06
Number of Experiments	1	1	1	1	2	2	1	1	1	1

Table 3— Experimental design matrix: induced aligned fractures.

Fracture Type	Induced Fracture												
Fracture offset	Aligned												
Proppant size (mesh)	100				40/70				30/50				No prop.
Proppant loading (lbm/ft^2)	0.03	0.06	0.10	0.20	0.03	0.06	0.10	0.20	0.03	0.06	0.10	0.20	-
Number of Experiments	-	5	6	-	-	4	1	-	-	1	1	-	7

Table 4— Experimental design matrix: induced displaced fractures.

Fracture Type	Induced Fracture												
Fracture offset	Displaced												
Proppant size (mesh)	100				40/70				30/50				No prop.
Proppant loading (lbm/ft^2)	0.03	0.06	0.10	0.20	0.03	0.06	0.10	0.20	0.03	0.06	0.10	0.20	-
Number of Experiments	1	2	2	1	1	3	1	1	1	1	1	1	6

3.1 Conductivity of natural fractures

The Barnett shale is a highly fractured reservoir. During the process of slickwater fracturing many of the natural fractures are reactivated and connected to the hydraulically induced complex fracture network. It is important to understand the potential conductivity of the natural fractures because they may significantly contribute to well productivity.

3.1.1 Conductivity of unpropped natural fractures

The natural fracture conductivity was measured using samples with well-cemented and poorly-cemented fractures. The poorly-cemented fractures were separated into two main categories based on the initial amount of cementing material: (1) fully-filled and (2) partially-filled fractures. The conductivity of those fractures was measured initially with the cementing material in place. After the measurements the infill was removed and the conductivity measured again. There was no consistency between the conductivity values of each fracture category due to the highly variable surface topography of each fracture.

The results from the measurements are presented in **Fig. 24.** The conductivity of the well-cemented fracture simulated a case of a non-reactivated fracture and served as a base line. There was only one shale sample that contained a fracture of this type. The conductivity at 3, 000 psi closure stress was 0.4 md-ft. The change of slope between 2,000 and 3,000 psi indicated that the anhydrite in the fracture underwent mechanical failure which resulted in fracture width reduction and lower measured conductivity.

The poorly-cemented fracture case simulates a hydraulically reactivated natural fracture where the cementing material was fully or partially removed due to mechanical failure or erosion caused by the high-velocity slurry during a fracturing operation. The conductivity was represented by six successful experimental measurements. On average, the conductivity was one order of magnitude higher than the conductivity of a well-cemented fracture. The values varied greatly mostly at lower closure stresses. The average conductivity at 4,000 psi closure stress was 0.9 md-ft with a standard deviation of 0.9 md-ft.

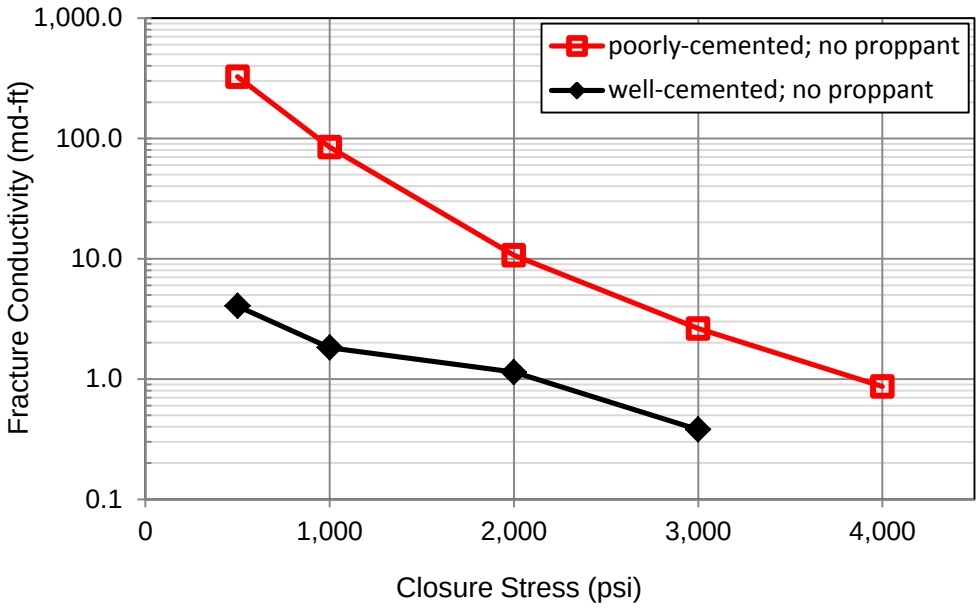

Fig. 24 – Conductivity of unpropped natural fractures

3.1.2 Conductivity of propped well-cemented natural fractures

The well-cemented fracture was carefully split apart and the cementing material removed. The conductivity was measured in the presence of 100-mesh white sand at 0.06 lb/ft^2 areal concentration. **Fig. 25** shows a comparison between the propped and unpropped well-cemented fracture conductivity. The sand performed much better as proppant than the cementing material by significantly increasing the fracture conductivity by one order of magnitude. The propped fracture conductivity at 4,000 psi was 3.2 md-ft or more than three times higher than the average poorly-cemented fracture conductivity (0.9 md-ft).

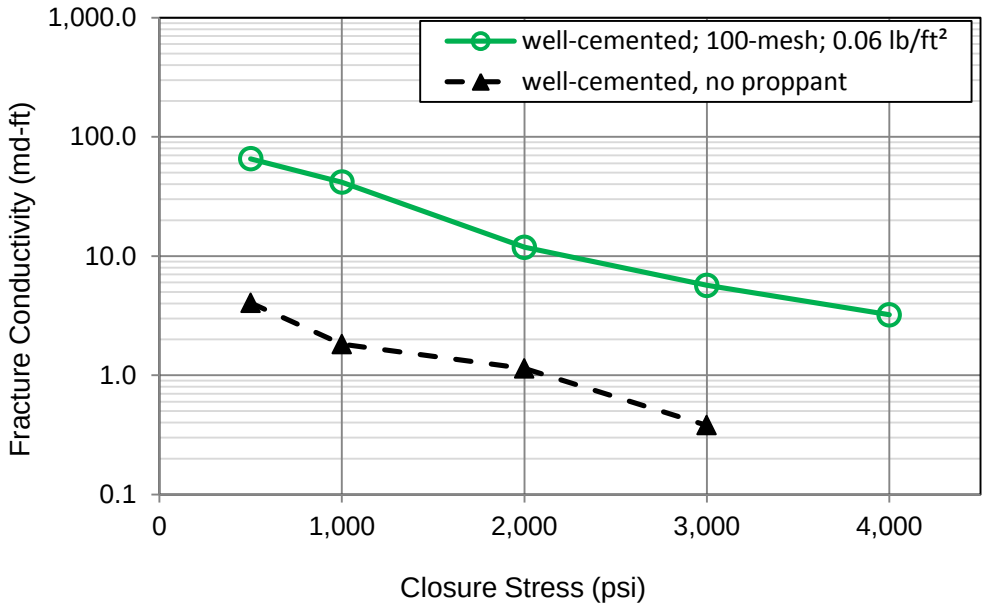

Fig. 25 – Conductivity of propped and unpropped well-cemented natural fracture

3.1.3 Conductivity of propped poorly-cemented natural fractures

The cementing material in the poorly-cemented natural fractures was removed after the initial unpropped conductivity measurements. The conductivity of a fully-filled and partially-filled fracture was measured using 100-mesh and 40/70-mesh white sand at 0.06 lb/ft^2. The average conductivity was calculated from two 100-mesh and two 40/70-mesh propped fracture cases. **Fig. 26** shows a plot of the average propped conductivity curves compared to the average unpropped poorly-cemented fracture conductivity. At a closure stress of 4,000 psi, the fracture propped with 100-mesh had an average conductivity of 14 md-ft with a standard deviation of 4.5 md-ft. This is more than one order of magnitude higher than the unpropped case (0.9 md-ft). The fracture propped with 40/70-mesh sand had the highest conductivity which was on average 37 md-ft with a standard deviation of 12 md-ft. The proppant kept the fracture open and was more resistant to crushing and compression compared with the natural cementing anhydrite material. This was observed from the slope of the propped and unpropped conductivity curves. The unpropped poorly-cemented graph decreases at a rate of ~0.67 log cycles per 1,000 psi closure stress, while the propped fracture conductivity decreases at a rate of 0.30 log cycles per 1,000 psi. The unpropped conductivity was higher than the 100-mesh propped fracture conductivity at closure stresses of 500 and 1,000 psi. This is because in the absence of proppant, there are residual interconnected void spaces within the fracture created by the non-matching rough surfaces. These voids have the potential to provide a more conductive path if they remain unpropped at low closure stresses.

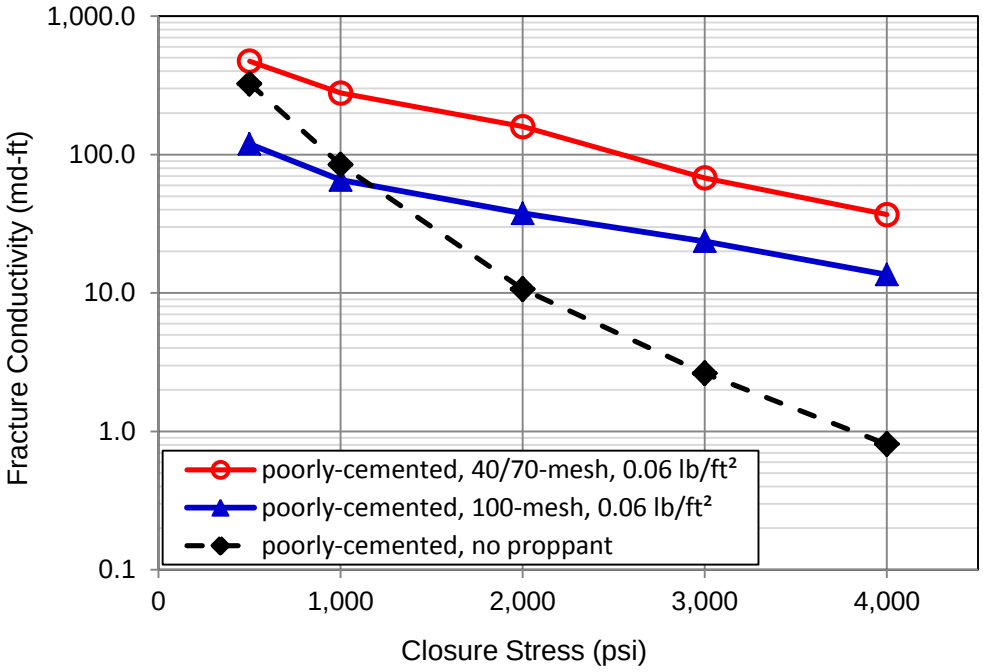

Fig. 26 – Average conductivity of propped and unpropped poorly-cemented natural fractures

3.2 Conductivity of unpropped induced fractures

Induced fractures were created along the bedding plane of the shale blocks. The resulting fracture surface was rough and resembled more closely the fracture wall of a real hydraulic fracture. Small debris and particles were possibly removed during the process of manually fracturing the rock. Some of the surfaces were offset by 0.1 in. to mimic the effect of shear displacement of the fracture walls during a field treatment. The displaced fractures had non-matching surfaces which created residual apertures within the fracture that could serve as conductive paths.

3.2.1 Comparison of aligned and displaced fracture conductivity in the absence of proppant

Multiple conductivity measurements were performed using aligned and displaced fractures in the absence of proppant. **Fig. 27** shows a comparison between the average of seven aligned and six displaced fracture conductivity measurements. Displaced fractures provided on average conductivity one order of magnitude higher compared to aligned fractures. The perfectly aligned fractures were conductive due to the presence of residual microscopic apertures within the fracture that resulted from the removal of microscopic debris from the fracture face when the fracture was induced along the shale bedding plane. The average unpropped aligned fracture conductivity at 3,000 psi closure stress was calculated to be 0.03 md-ft with a standard deviation of 0.1 md-ft (based only two available measurements at this stress level). The average unpropped displaced fracture conductivity at a closure stress of 3,000 psi was 2.7 md-ft with a standard deviation of 4.1 md-ft (based on six measurements). The conductivity at 4,000 psi closure stress was based on four measurements and was calculated to be 0.9 md-ft with a standard deviation of 1.2 md-ft. All shale samples had different fracture surfaces. The large standard deviations of conductivity values were most likely due to the different asperities distribution on the fracture surface and the various degree of aperture connectivity within the fracture.

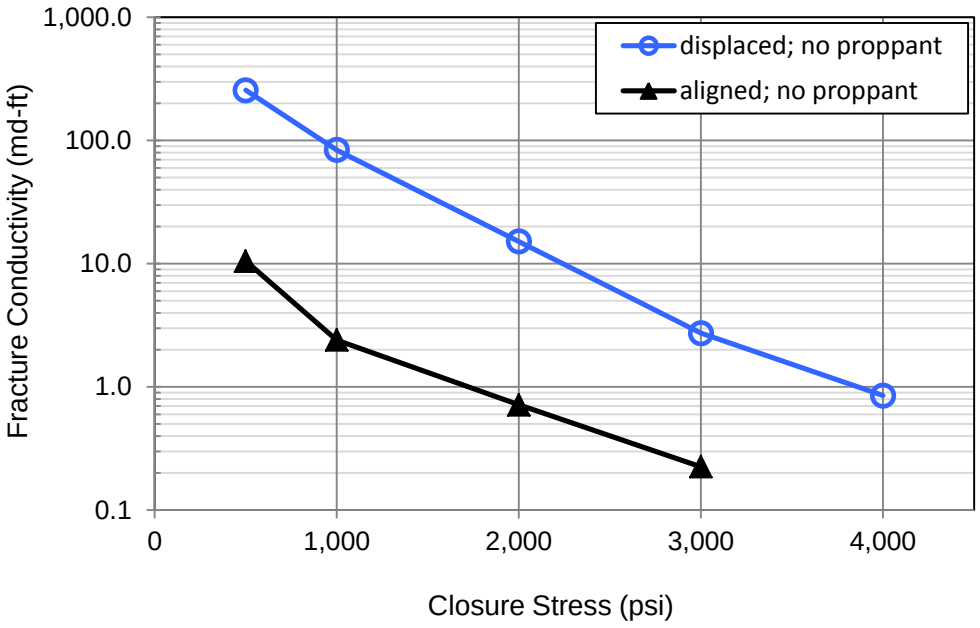

Fig. 27 – Average conductivity of unpropped induced fractures

3.2.2 Comparison of natural and induced fracture conductivity in the absence of proppant

The average unpropped conductivity of aligned fractures was similar to that of well-cemented fractures. The slightly higher well-cemented fracture conductivity (0.4 md-ft compared to 0.2 at 3,000 psi) could be attributed to the infill material that acts like very low permeability proppant. The comparison is shown in **Fig. 28**.

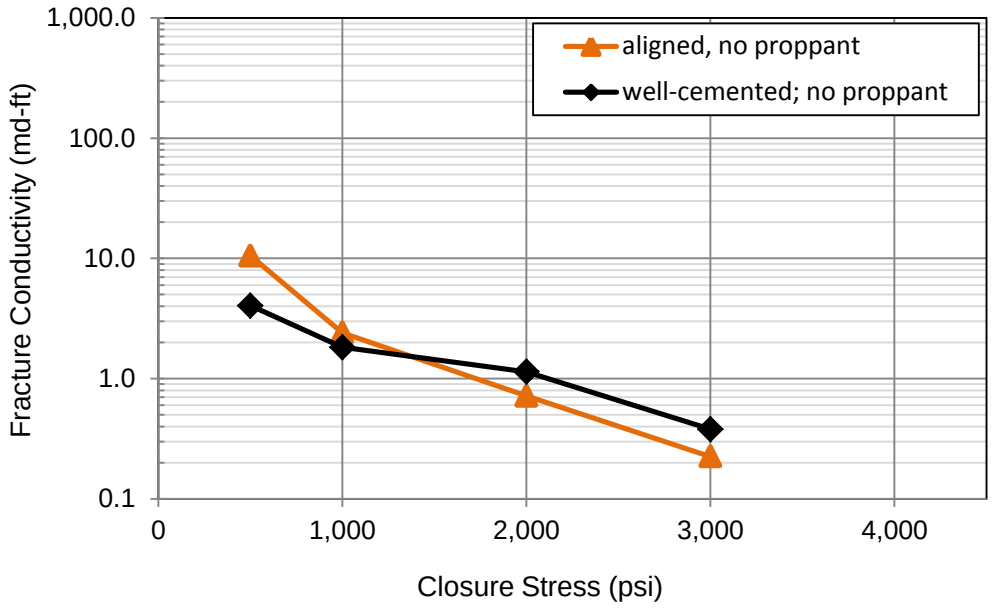

Fig. 28 – Comparison of average conductivity of unpropped aligned and well-cemented fractures

Interestingly, the average displaced and poorly-cemented induced fracture conductivity values were very similar at low and high closure stress levels (**Fig. 29**). These types of fractures have one common characteristic – a highly variable fracture surface topography. The average displaced fracture conductivity at 4,000 psi was 0.9 md-ft (four measurements) with a standard deviation of 1.2 md-ft. The average poorly cemented fracture conductivity was measured to be 0.9 md-ft (five measurements) with a standard deviation of 0.9 md-ft. The average conductivity and standard deviations were very close at a high closure stress.

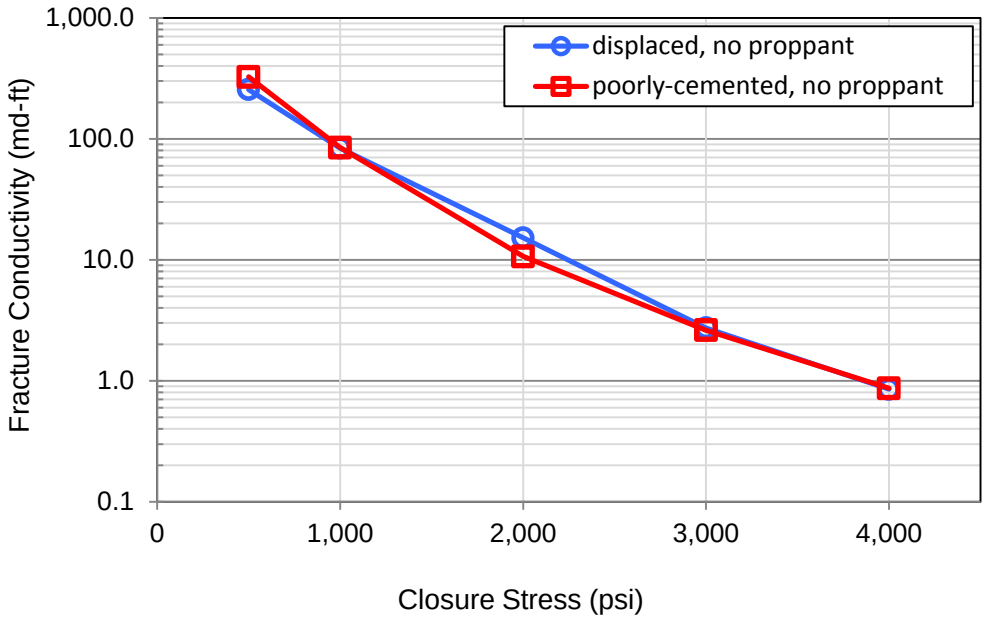

Fig. 29 – Comparison of average conductivity of unpropped displaced and poorly-cemented fractures

3.3 The effect of proppant size on induced fracture conductivity

The effect of proppant size on fracture conductivity was studied in the induced fractures. For the purpose of this experiment white sand of 100-mesh, 40/70-mesh and 30/50 mesh was used. Some of the conductivity curves represent average values. **Table 5** shows details on each measurement.

Table 5 – Summary of conductivity measurements of propped aligned and displaced fracture

Fracture Type	Proppant loading [lb/ft2]	Proppant mesh size	Count	Average conductivity at 4,000 psi [md-ft]	Standard deviation [md-ft]
Aligned	No proppant	n/a	7	0.23	0.09
	0.06	100	5	5.32	2.27
		40/70	4	21.96	5.50
		30/50	1	50.09	n/a
	0.1	100	6	14.31	6.58
		40/70	1	46.44	n/a
		30/50	1	88.63	n/a
Displaced	No proppant	n/a	6	0.85	1.17
	0.06	100	2	8.83	4.99
		40/70	3	25.39	13.84
		30/50	1	38.81	n/a
	0.1	100	2	12.45	5.06
		40/70	1	42.16	n/a
		30/50	1	58.23	n/a

3.3.1 Conductivity of propped aligned fractures

The average conductivity of aligned fractures containing 100-mesh, 40/70-mesh and 30/50 mesh sand at loadings of 0.06 lb/ft^2 and 0.10 lb/ft^2 was compared to the average unpropped aligned fracture conductivity in **Figs. 30** and **31.** The propped conductivity was significantly higher and increased with proppant size. The proppant maintained the fracture conductivity more effectively at higher closure stresses. The slope of the propped fracture with 0.06 lb/ft^2 of sand was slightly steeper (0.30 log cycle

per 1,000 psi) compared to the case with 0.10 lb/ft^2 sand loading (0.24 log cycle per 1,000 psi). Higher proppant concentrations provided better resistance to closure stress which results in a smaller reduction in fracture width. At 4,000 psi closure stress the conductivity of 100-mesh, 40/70-mesh and 30/50 mesh sand at 0.06 lb/ft^2 was 5.3 md-ft, 22 md-ft, and 50 md-ft respectively. The conductivity at 0.10 lb/ft^2 loading was 14 md-ft, 46 md-ft, and 89 md-ft respectively. The presence of proppant in the fractures increased conductivity with at least almost two orders of magnitude compared to the unpropped case.

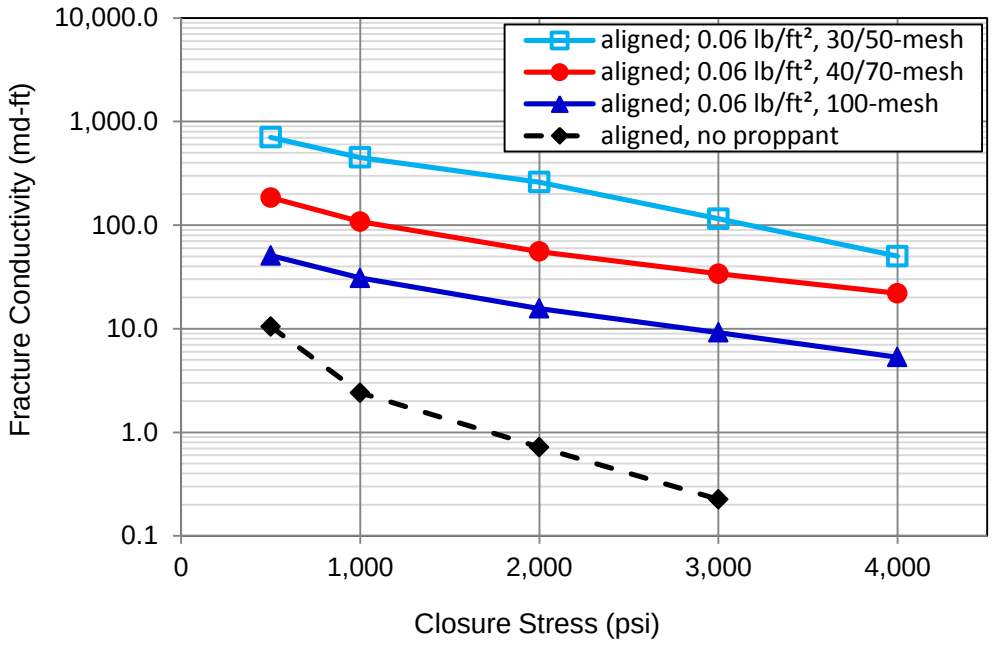

Fig. 30 – Comparison of unpropped and propped aligned fracture conductivity with 100-mesh, 40/70-mesh, and 30/50-mesh sand at 0.06 lb/ft^2 proppant loading

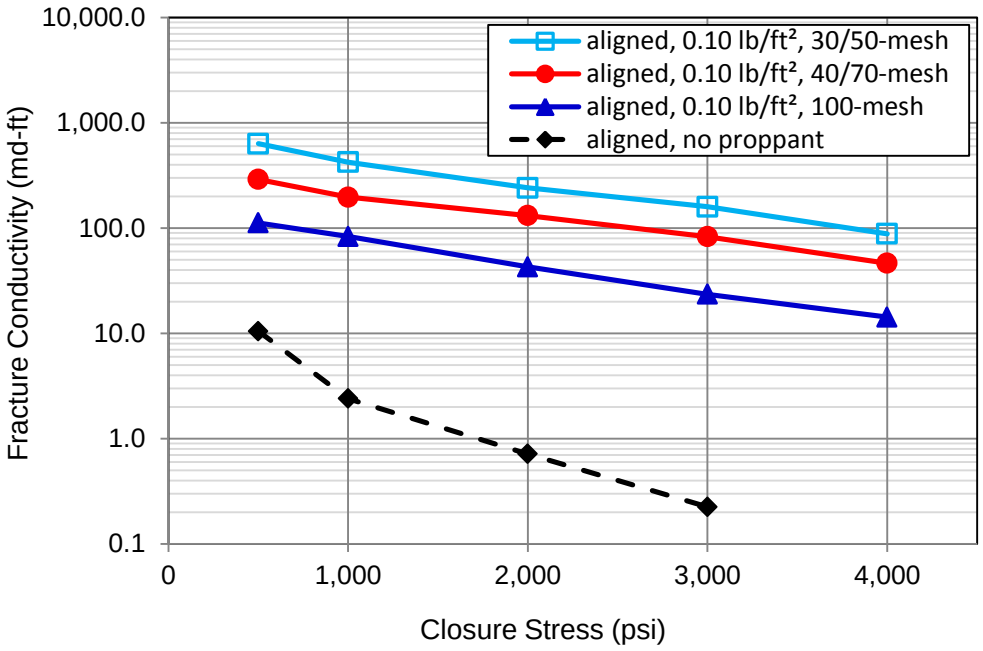

Fig. 31 –Comparison of unpropped and propped aligned fracture conductivity with 100-mesh, 40/70-mesh, and 30/50-mesh sand at 0.10 lb/ft^2 proppant loading

3.3.2 Conductivity of propped displaced fractures

The average conductivity of displaced fractures propped with 100-mesh, 40/70-mesh and 30/50 mesh sand at loadings of 0.06 lb/ft^2 and 0.10 lb/ft^2 was compared to the average unpropped displaced fracture conductivity in **Figs. 32** and **33.** The propped conductivity was at least one order of magnitude (100-mesh sand) higher than the unpropped conductivity at 4,000 psi closure stress. At lower stresses (500 and 1,000 psi) the average conductivity of unpropped fractures was higher than the that of fractures propped with 100-mesh sand. This is because the interconnected apertures in the displaced fractures are less conductive if proppant is present. However, as the closure stress increased, the contact points that kept the unpropped displaced fracture open

began to compress and possibly deform. As a result, the residual void spaces in the fracture became smaller and less interconnected which ultimately lead to reduced conductivity. At higher closure stress the permeable proppant pack could maintain the fracture width and provide higher conductivity.

Similarly to aligned propped fractures, the slope of the propped displaced fracture with 0.06 lb/ft^2 of sand was steeper on average (0.33 log cycle per 1,000 psi) compared to the case with 0.10 lb/ft^2 sand loading (0.27 log cycle per 1,000 psi). The proppant provided a better conductive path if it was placed at higher concentrations. The conductivity of 100-mesh, 40/70-mesh and 30/50 mesh sand at 0.06 lb/ft^2 at 4,000 psi closure stress was measured to be 8.8 md-ft, 25 md-ft, and 38 md-ft respectively. The conductivity values at 0.10 lb/ft^2 loading at 4,000 psi closure stress were 12 md-ft, 42 md-ft, and 58 md-ft respectively. The sudden change in the slope of the conductivity curve of the fracture propped with 30/50-mesh sand at 0.06 lb/ft^2 was a result of the effect of partial monolayer. It could not withstand high closure stress which resulted in lower fracture conductivity due to fracture width reduction. This is further investigated in section 3.3.4 and 3.3.5.

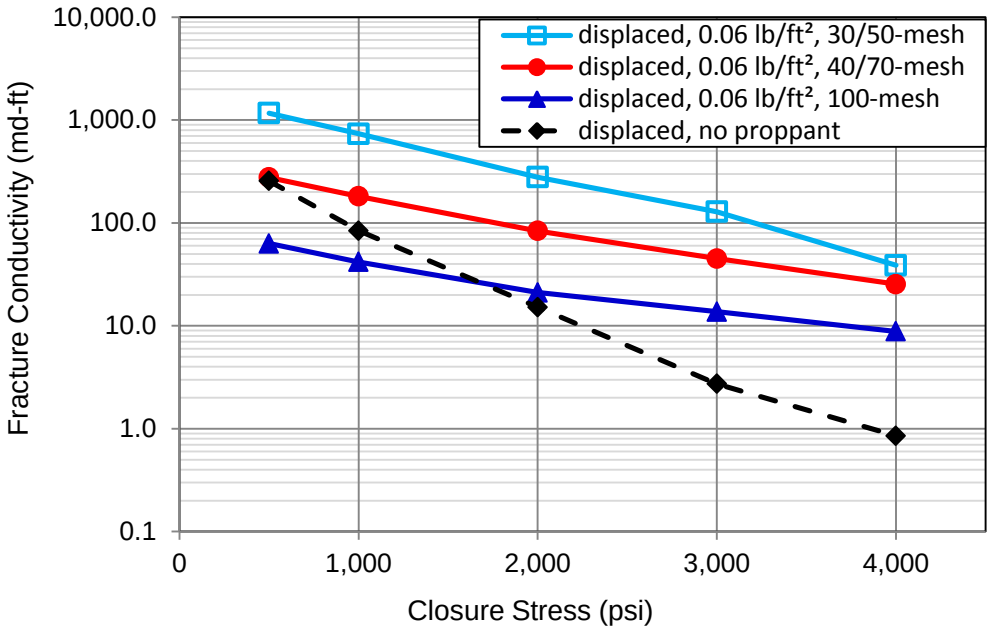

Fig. 32 – Comparison of unpropped and propped displaced fracture conductivity with 100-mesh, 40/70-mesh, and 30/50-mesh sand at 0.06 lb/ft^2 proppant loading

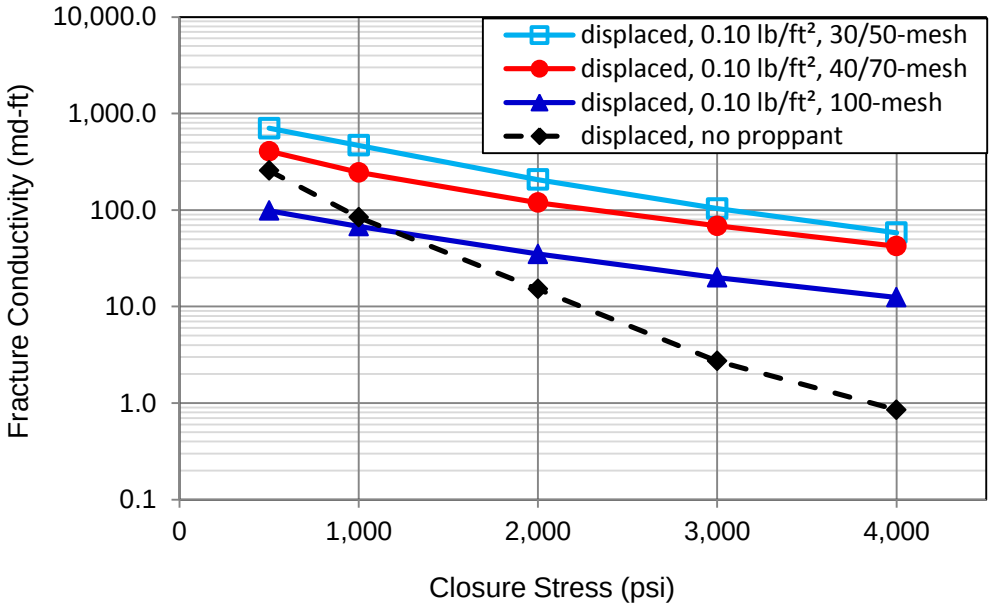

Fig. 33 – Comparison of unpropped and propped displaced fracture conductivity with 100-mesh, 40/70-mesh, and 30/50-mesh sand at 0.10 lb/ft^2 proppant loading

3.3.3 Comparison of aligned and displaced fracture conductivity in the presence of proppant

The conductivity of propped aligned and displaced fractures was compared using 100-mesh, 40/70-mesh and 30/50-mesh white sand at low areal proppant loadings of 0.06 lb/ft^2 and 0.10 lb/ft^2. The average conductivity of aligned fracture seemed to be slightly higher in some of the cases. It is important to mention that the samples with aligned and displaced fracture surfaces represented different core samples with different fracture surface characteristics.

Figures 34 through 39 show that if proppant was introduced in the induced fracture, even at low concentrations, the conductivity became proppant-dominated. The fact that the conductivity values of propped displaced and aligned fractures were fairly similar suggested that proppant was the dominant contributor to fracture conductivity in propped fractures. The conductivity was weakly dependent on the degree of fracture roughness or displacement.

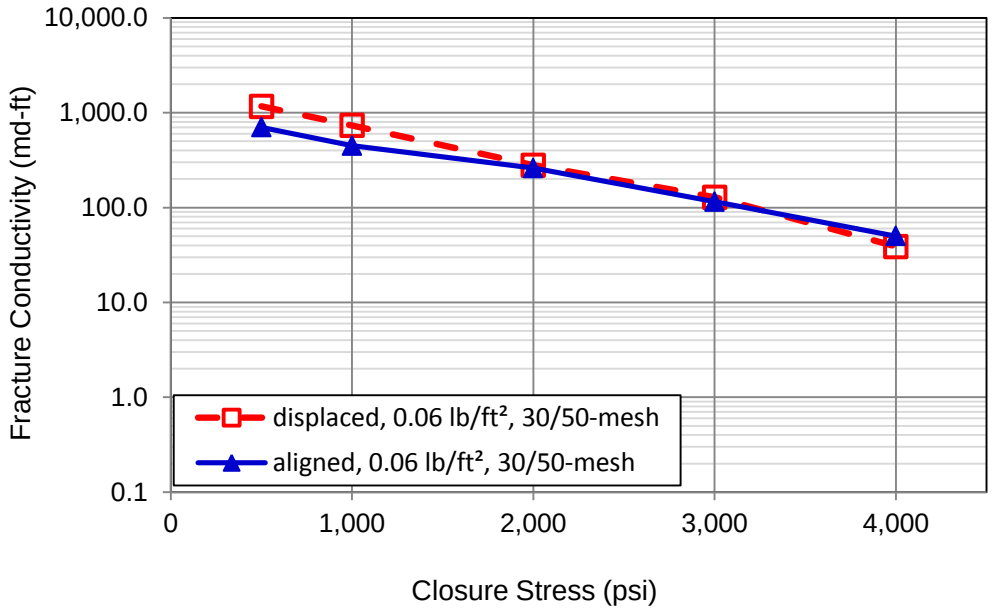

Fig. 34 – Comparison of displaced and aligned fracture conductivity with 0.06 lb/ft^2 of 30/50-mesh white sand

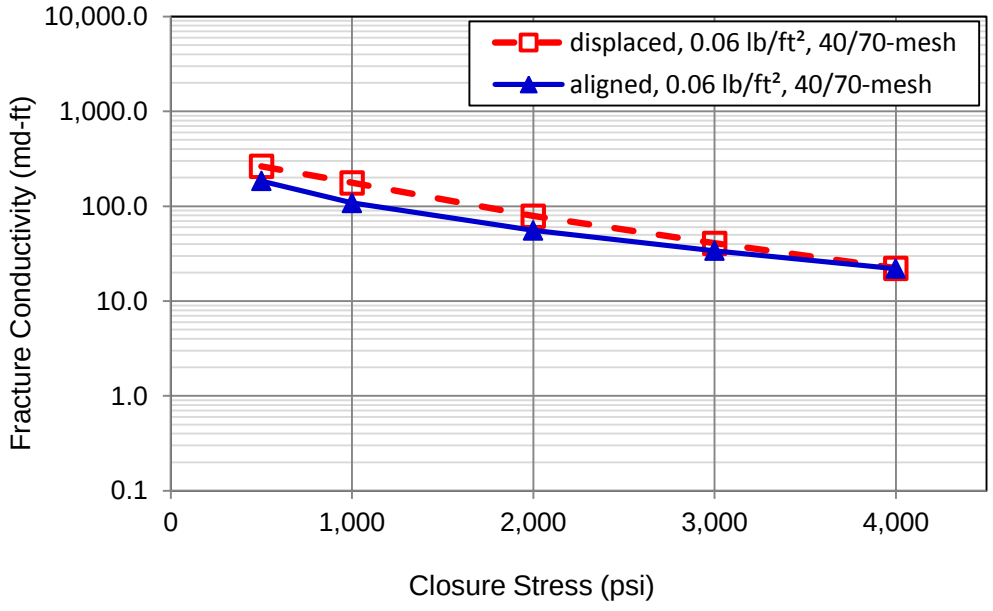

Fig. 35– Comparison of displaced and aligned fracture conductivity with 0.06 lb/ft^2 of 40/70-mesh white sand

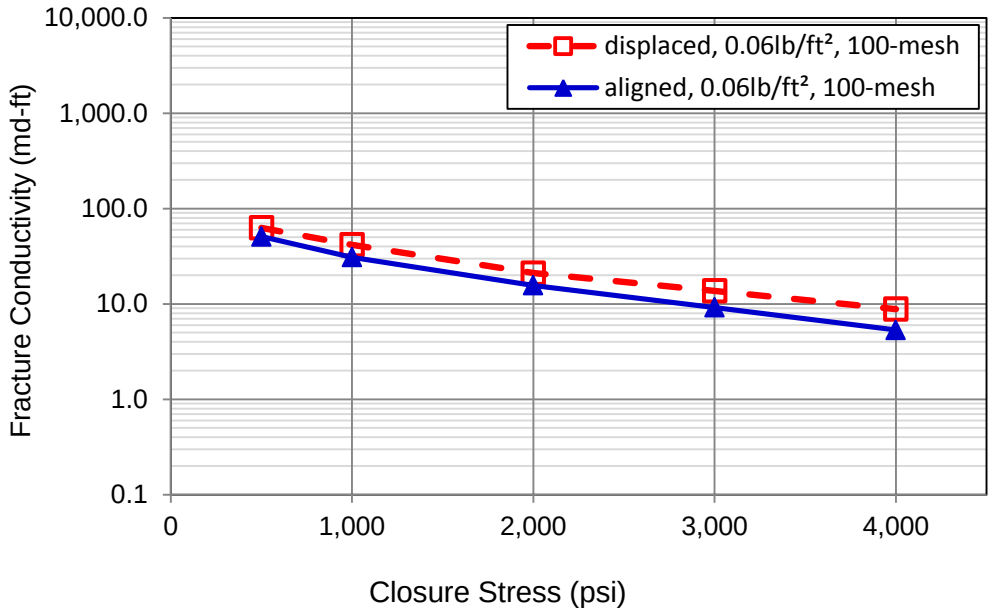

Fig. 36– Comparison of displaced and aligned fracture conductivity with 0.06 lb/ft^2 of 100-mesh white sand

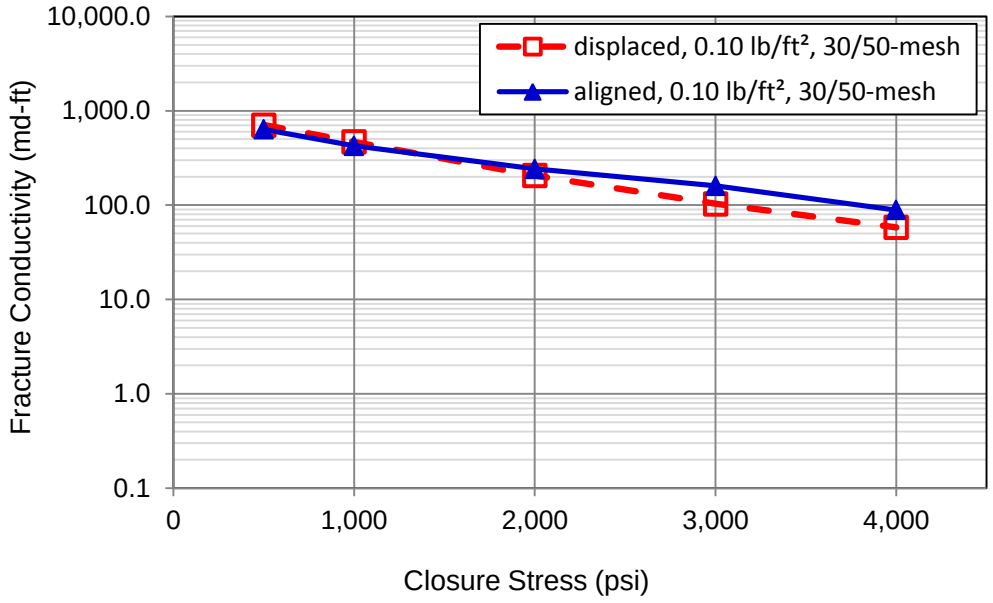

Fig. 37– Comparison of displaced and aligned fracture conductivity with 0.10 lb/ft^2 of 30/50-mesh white sand

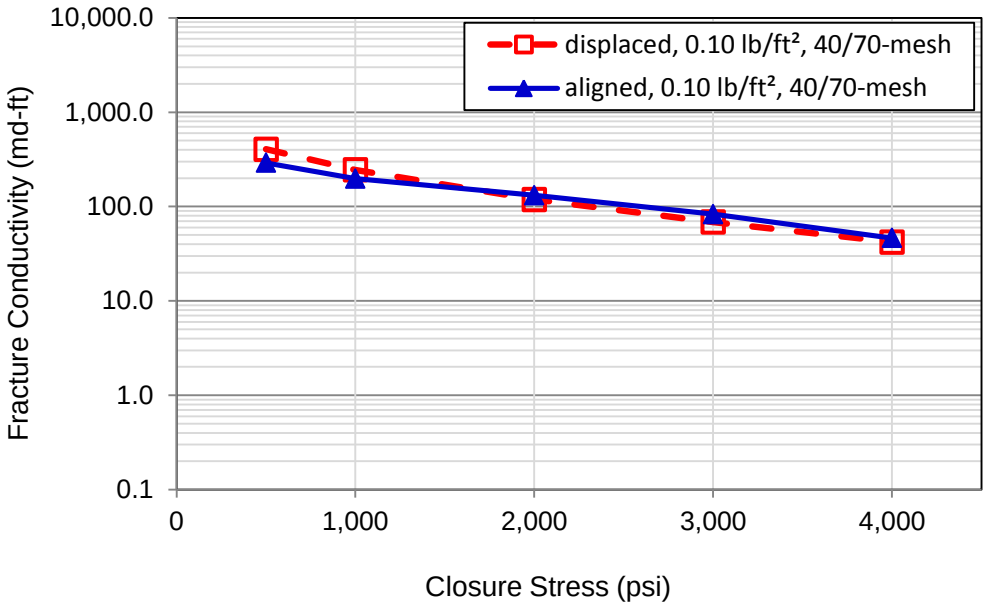

Fig. 38– Comparison of displaced and aligned fracture conductivity with 0.10 lb/ft^2 of 40/70-mesh white sand

Fig. 39– Comparison of displaced and aligned fracture conductivity with 0.10 lb/ft^2 of 100-mesh white sand

3.4 The effect of proppant concentration on induced fracture conductivity

Section 3.3.3 discussed the role of low proppant concentrations in aligned and displaced fracture. The results showed that propped fracture conductivity is proppant-dominated and not greatly affected by the fracture surface roughness. Furthermore, a more realistic representation of a real Barnett shale fracture would be one with offset fracture faces and non-matching surfaces. Therefore, series of conductivity experiments were performed using displaced fractures to study the effect of proppant loading on fracture conductivity. To clearly identify the effect of ultra-low to medium proppant loadings on fracture conductivity, white sand of 100-mesh, 40/70-mesh, and 30/50-mesh size was placed in displaced fractures at areal concentrations of 0.03 lb/ft^2, 0.10 lb/ft^2, and 0.20 lb/ft^2. All three conductivity measurements were performed with a single shale core sample to fully eliminate the effect of fracture surface roughness which could be significant at ultra-low proppant concentrations (0.03 lb/ft^2). A summary of the results discussed in section 3.4 is presented in **Table 6**.

Table 6 – Summary of propped displaced fracture conductivity

Mesh size	Concentration [lb/ft²]	Conductivity reduction rate [log cycle per 1,000 psi]	Conductivity at 4,000 psi [md-ft]
100	0.03 lb/ft²	0.30	39.3
	0.10 lb/ft²	0.10	16.0
	0.20 lb/ft²	0.27	2.80
40/70	0.03 lb/ft²	0.40	15.7
	0.10 lb/ft²	0.31	42.2
	0.20 lb/ft²	0.17	82.2
30/50	0.03 lb/ft²	0.50	20.8
	0.10 lb/ft²	0.30	58.2
	0.20 lb/ft²	0.13	134.1

3.4.1 Conductivity of propped displaced fractures

The results from the laboratory measurements using displaced fractures are shown in **Figs. 43 through 45**. The propped fracture conductivity increased with higher proppant concentration. This trend was observed for all proppant sizes at 4,000 psi. The same trend did not fully apply for areal concentrations of 0.03 lb/ft^2 of 40/70-mesh and 30/50-mesh sand when a partial proppant monolayer was formed in the fracture. It provided high conductivity at lower closure stresses but it failed to maintain the conductivity as the closure stress was increased. As a result the conductivity sharply decreased.

It is important to note that 100-mesh sand at 0.03 lb/ft^2 loading did not form a partial monolayer because the small grain size which resulted in large number of particles per unit weight. This is also indicated by the behavior of the conductivity curves shown on **Fig. 44**. The conductivity increased at all closure stress levels with higher proppant loading.

The slight change of the slope of the conductivity curve of 100-mesh sand at 0.20 lb/ft^2 between 3,000 and 4,000 psi could be attributed to a greater degree of compaction and rearrangement of the sand in the proppant pack at high stress levels. The effect of compaction would be more accentuated in a proppant pack that contains a large number of small particles (i.e. 100-mesh at 0.20 lb/ft^2). The conductivity decline rates at concentrations of 0.03 lb/ft^2, 0.10 lb/ft^2, 0.20 lb/ft^2 were 0.30, 0.10, and 0.27 log cycle per 1,000 psi respectively. This was counter intuitive because the higher proppant concentrations (more grain layers in the proppant pack) should be more resistant to

closure stress and provide a slower rate of fracture width reduction (the trend observed for 40/70-mesh and 30/50-mesh sand). This did not apply for 100-mesh sand within the range of proppant areal concentration used in this study. Although 100-mesh sand did not form a partial monolayer in the fracture at a proppant loading of 0.03 lb/ft^2, it tended to settle in the valleys of the fracture surface leaving the peaks uncovered. Therefore, the fracture was kept open initially by the rock contact points (similar to the unpropped case). **Fig. 40** shows that at elevated stresses the rock at the contact points was compressed and the proppant in the valleys started acting against the closure stress. The combined effect of proppant and rock contact points provided a lower rate of fracture conductivity reduction than the unpropped case (0.25 log cycle per 1,000 psi).

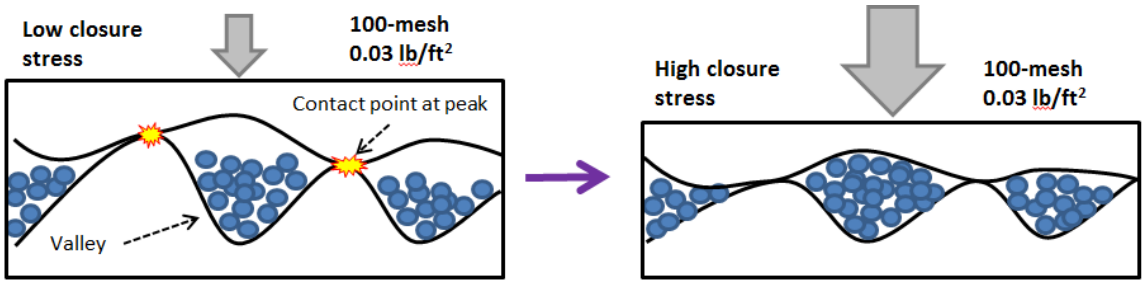

Fig. 40– Schematic of 100-mesh sand distribution in a displaced induced fracture at concentration of 0.03 lb/ft^2

When the fracture was propped with 0.10 lb/ft^2 of 100-mesh sand, not only the valleys but also a lot of the smaller peaks along the surface were covered by sand. Therefore, the fracture width change was affected predominantly by the proppant and

not by the mechanical properties of the rock contact points (**Fig. 41**). This is why the conductivity decline rate was lower in this case (0.10 log cycle per 1,000 psi).

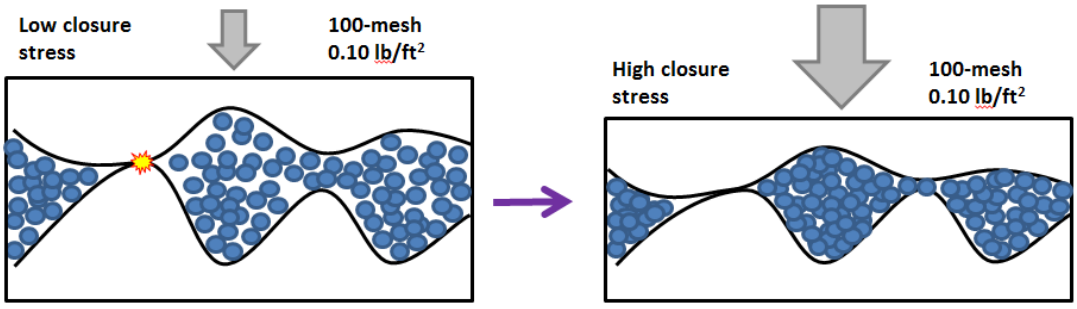

Fig. 41 – Schematic of 100-mesh sand distribution in a displaced induced fracture at concentration of 0.10 lb/ft^2

Higher proppant loadings of 0.20 lb/ft^2 fully covered the fracture surface irregularities (**Fig. 42**). The increase of conductivity decline rate from 0.10 to 0.27 log cycle per 1,000 psi could be attributed to compaction and rearrangement of the grains in the proppant pack. Compaction and rearrangement is usually more emphasized in proppant packs with more grain layers. Larger grains weigh more which results in a smaller number of grains per unit weight. This is why this was not observed for larger sand size particles (40/70-mesh and 30/50-mesh) at this concentration due to the smaller number of particle layers. This study did not include conductivity measurements at concentrations higher than 0.20 lb/ft^2.

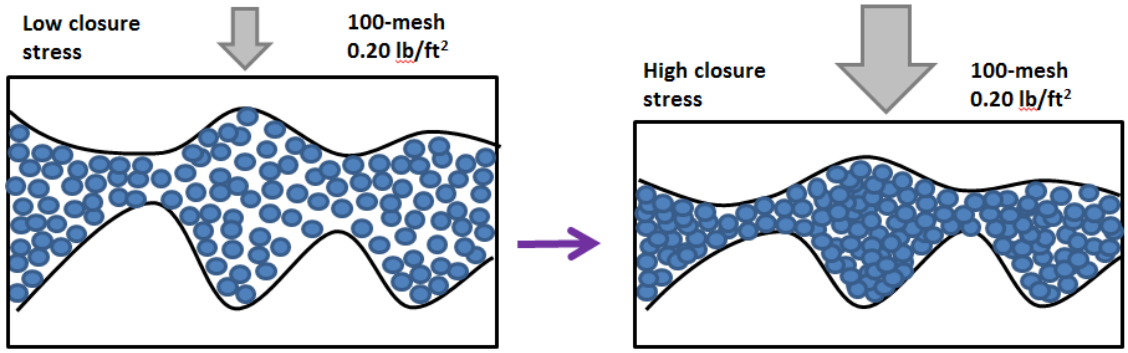

Fig. 42 – Schematic of 100-mesh sand distribution in a displaced induced fracture at concentration of 0.20 lb/ft^2

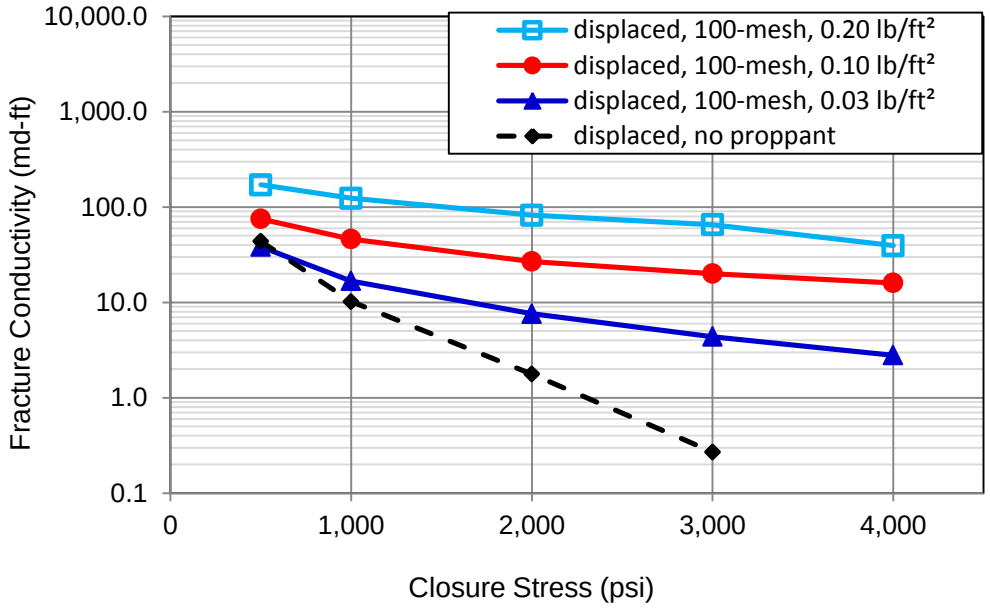

Fig. 43 – Conductivity of unpropped and propped displaced fracture conductivity with 100-mesh sand at 0.03 lb/ft^2, 0.10 lb/ft^2 , 0.20 lb/ft^2 proppant loading

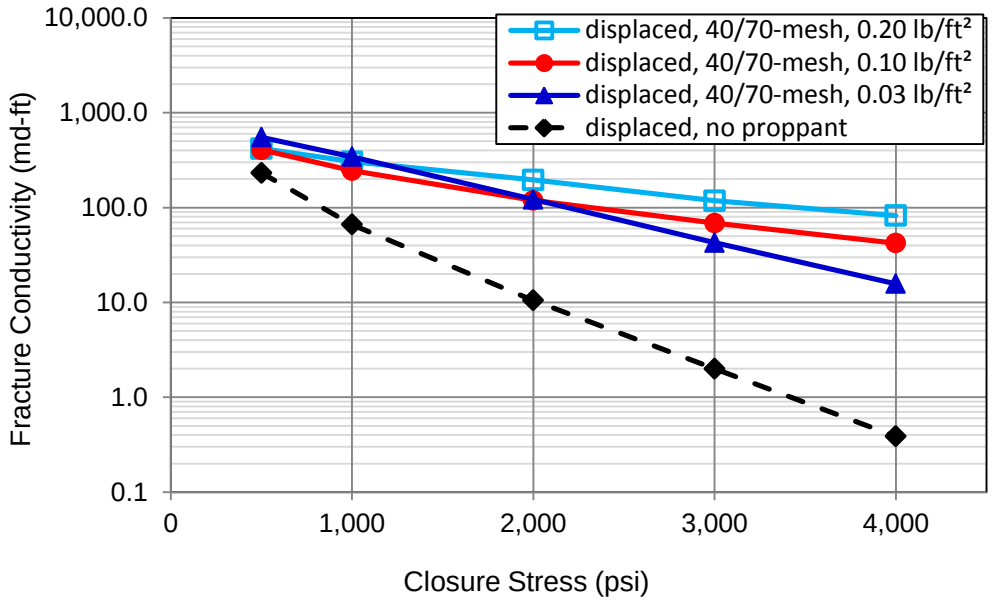

Fig. 44 – Conductivity of unpropped and propped displaced fracture conductivity with 40/70-mesh sand at 0.03 lb/ft^2, 0.10 lb/ft^2 , 0.20 lb/ft^2 proppant loading

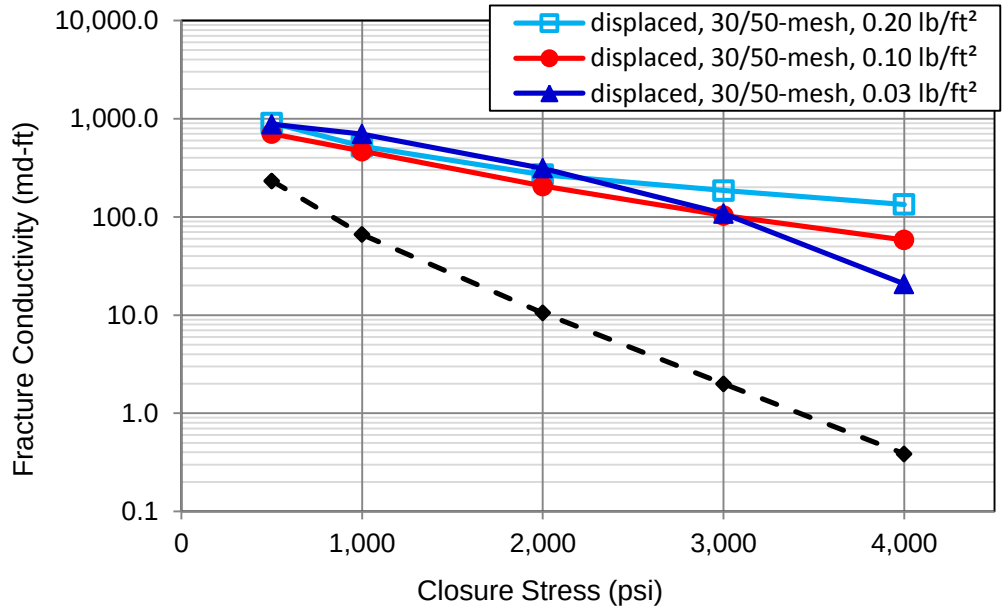

Fig. 45 – Conductivity of unpropped and propped displaced fracture conductivity with 30/50-mesh sand at 0.03 lb/ft^2, 0.10 lb/ft^2 , 0.20 lb/ft^2 proppant loading

The conductivity results shown in **Figs. 43 through 45** were plotted as a function of proppant concentration in **Figs. 46 through 48**. At lower closure stresses and low proppant concentrations (0.03 lb/ft^2) the conductivity of fractures propped with larger sand (40/70-mesh and 30/50-mesh) exhibited higher values than the conductivity of fractures propped with higher proppant loadings of 0.10 lb/ft^2 and 0.20 lb/ft^2 (multiple layers of proppant). The partial monolayer effect was more emphasized with larger proppant grain size (30/50-mesh).

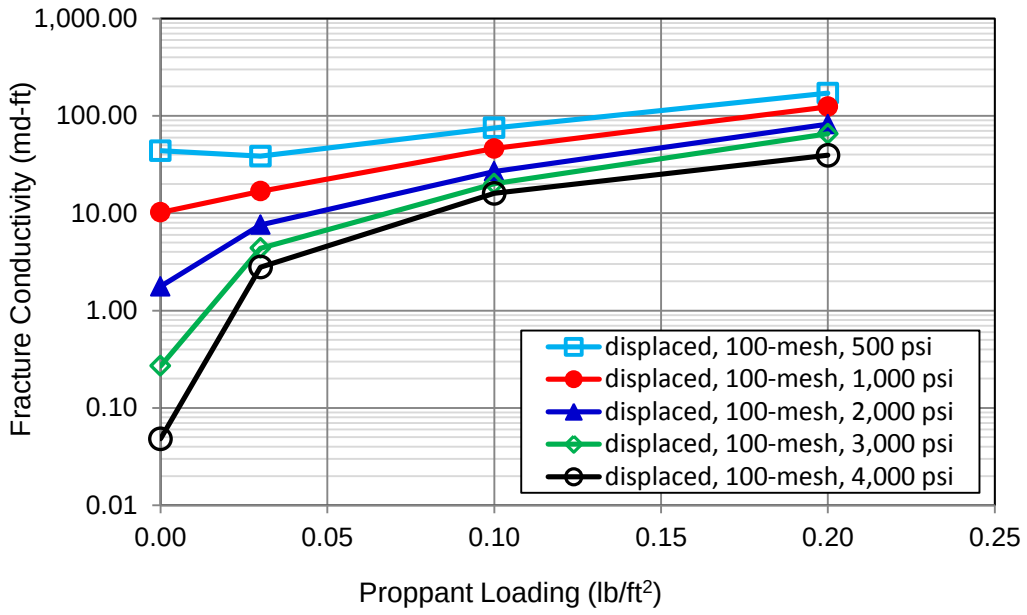

Fig. 46 – Conductivity of displaced fracture propped with 100-mesh sand as a function of proppant areal concentration

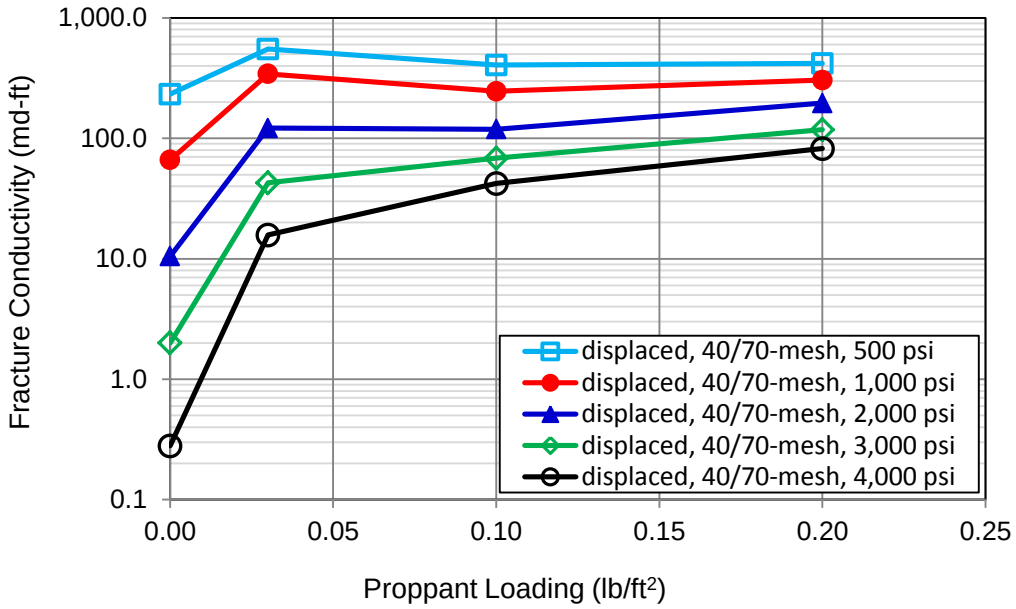

Fig. 47– Conductivity of displaced fracture propped with 40/70-mesh sand as a function of proppant areal concentration

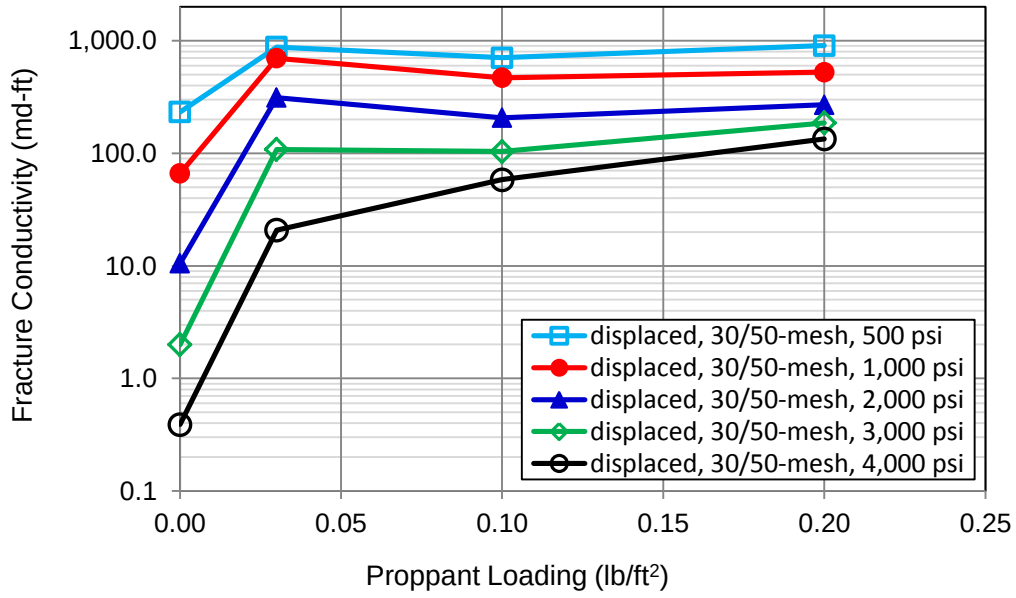

Fig. 48 – Conductivity of displaced fracture propped with 30/50-mesh sand as a function of proppant areal concentration

3.4.2 Conductivity of displaced fractures propped with a partial monolayer of sand

To carefully study the effect of a partial monolayer in greater detail conductivity measurements were performed with particles with uniform size. Proppant with narrow grain size distribution was sampled from the 30/50-mesh sand. Only grains retained in the 40-mesh sieve during the sieve analysis were used. The 30/40-mesh proppant was placed in a displaced fracture and the conductivity was measured using areal concentrations of 0.03 lb/ft^2 and 0.20 lb/ft^2.

Figure 49 shows similar observations to those presented in section 3.3.4. The 30/40-mesh proppant partial monolayer (0.03 lb/ft^2) performed better than the proppant pack (0.20 lb/ft^2) at lower closure stresses (< 3,000 psi). However, the proppant pack provided much higher conductivity (98 md-ft) at a closure stress of 4,000 psi or about three times higher than the conductivity of the proppant monolayer (32 md-ft). This is because the proppant pack is more resistant to the closure stress due to a more uniform stress distribution among the proppant grains. Furthermore, the multiple layers of sand grains in the proppant pack result in a much larger fracture width compared to the monolayer case. Overall, the proppant monolayer provided a conductivity two orders of magnitude higher than the conductivity of the unpropped case (0.4 md-ft) at 4,000 psi closure stress. The rate of conductivity reduction in the proppant pack was 0.14 log cycle per 1,000 psi or about 3.5 times lower than the rate of conductivity reduction in the

monolayer case (0.5 log cycle per 1,000 psi) or ~6 times higher than the conductivity decline rate of the unpropped fracture (0.84 log cycle per 1,000 psi).

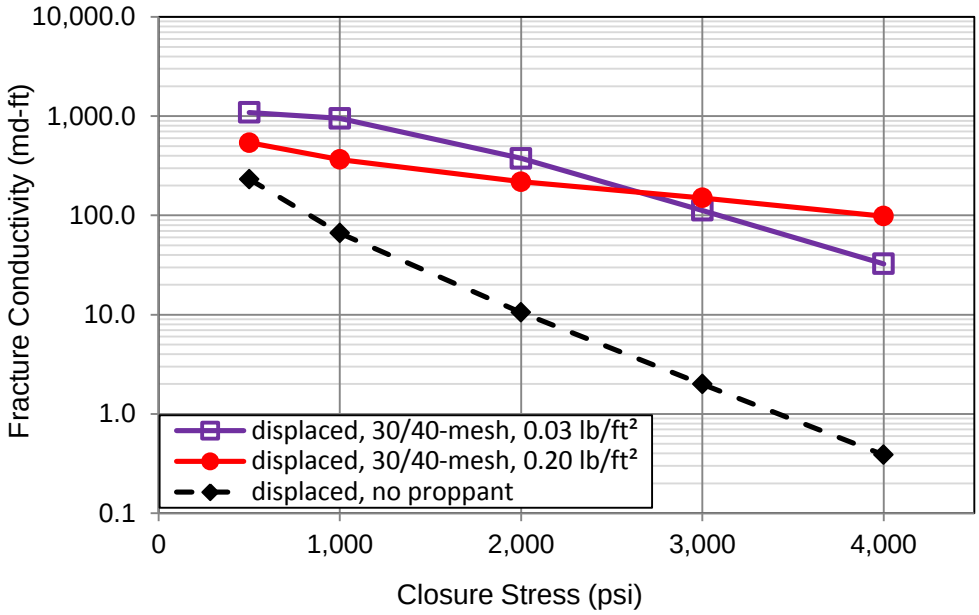

Fig. 49 – Conductivity of unpropped and propped displaced fracture conductivity with 30/40-mesh sand at 0.03 lb/ft^2, 0.20 lb/ft^2 proppant loading

4. CONCLUSIONS AND RECOMMENDATIONS

4.1 Conclusions

This study presented the results from a series of short-term static conductivity measurements using real Barnett shale core samples. Natural and induced fracture conductivity was studied in the absence of proppant and at low proppant concentrations of 0.03 lb/ft^2 up to 0.20 lb/ft^2 using 100-mesh, 40/70-mesh, and 30/50-mesh white sand. The following conclusions and observations were made based on this experimental study:

1. Poorly-cemented natural fractures provide effective conductive pathways.
2. Unpropped fractures with perfectly aligned surfaces can be conductive.
3. Displaced fractures provide conductivity one order of magnitude higher than the conductivity of aligned fractures due to the residual apertures between the two non-matching fracture surfaces.
4. Propped fracture conductivity is proppant-dominated. It is less affected by the degree of fracture surface roughness or displacement.
5. The conductivity of propped fractures increases with larger proppant size and higher concentration within the limits of the experimental design of this study.
6. Larger proppant (40/70-mesh and 30/50-mesh) formed a partial monolayer at concentrations of 0.03 lb/ft^2 and 0.06 lb/ft^2 (30/50-mesh only). Even though the partial monolayer provided significant conductivity at low closure stresses, it failed to maintain the fracture conductivity at higher stress levels.

4.2 Recommendations

The short-term shale fracture conductivity experiments included in this study used dry nitrogen to measure conductivity. The shale fracture surface was not exposed to any fracturing fluids used in field treatments. Therefore, long-term dynamic conductivity measurements using fracturing fluids with realistic chemical composition would provide greater understanding of rock-fluid interactions and their effect on fracture conductivity.

REFERENCES

Awoleke, O., Romero, J., Zhu, D., Hill, A. D. (2012). Experimental Investigation of Propped Fracture Conductivity in Tight Gas Reservoirs Using Factorial Design. SPE Hydraulic Fracturing Technology Conference. The Woodlands, Texas, USA, Society of Petroleum Engineers.

Bandis, S. C., Lumsden, A. C., Barton, N.R. (1983). "Fundamentals of rock joint deformation." International Journal of Rock Mechanics and Mining Sciences & Geomechanics Abstracts 20(6): 249-268.

Barton, N. R., Bandis, S. C., Bakhtar, K. (1985). "Strength, deformation and conductivity coupling of rock joints." International Journal of Rock Mechanics and Mining Sciences & Geomechanics Abstracts 22(3): 121-140.

Branagan, P. T., Warpinski, N. R., Engler, B., Sandia National Laboratories, Wilmer, R. (1996). Measuring the Hydraulic Fracture-Induced Deformation of Reservoirs and Adjacent Rocks Employing a Deeply Buried Inclinometer Array: GRI/DOE Multi-Site Project. SPE Annual Technical Conference and Exhibition. Denver, Colorado, 1996 Copyright 1996, Society of Petroleum Engineers, Inc.

Brannon, H. D., Malone, M. R., Rickards, A. R., Wood, W. D., Edgeman, R., Bryant, J. L. (2004). Maximizing Fracture Conductivity with Proppant Partial Monolayers: Theoretical Curiosity or Highly Productive Reality? SPE Annual Technical Conference and Exhibition. Houston, Texas, Society of Petroleum Engineers.

Britt, L. K., Smith, M. B., Haddad, Z., Lawrence, P., Chipperfield, S., Hellman, T. (2006). Water-Fracs: We Do Need Proppant After All. SPE Annual Technical Conference and Exhibition. San Antonio, Texas, USA, Society of Petroleum Engineers.

Cooke Jr., C. E. (1973). "Conductivity of Fracture Proppants in Multiple Layers." Journal of Petroleum Technology 25(9): 1101-1107.

Cooke Jr., C. E. (1975). "Effect of Fracturing Fluids on Fracture Conductivity." Journal of Petroleum Technology 27(10): 1273-1282.

Coulter, G. R., Benton, E. G., Thompson, C. L. (2004). Water Fracs and Sand Quantity: A Barnett Shale Example. SPE Annual Technical Conference and Exhibition. Houston, Texas, Society of Petroleum Engineers.

Dam, D. B. v., Pater, C. J. d., Romjin, R.(1998). Analysis of Hydraulic Fracture Closure in Laboratory Experiments. SPE/ISRM Rock Mechanics in Petroleum Engineering. Trondheim, Norway, 1998 Copyright 1998, Society of Petroleum Engineers Inc.

Dam, D. B. v. Pater, C. J. d. (1999). Roughness of Hydraulic Fractures: The Importance of In-Situ Stress and Tip Processes. SPE Annual Technical Conference and Exhibition. Houston, Texas, Society of Petroleum Engineers.

Darin, S. R. and Huitt, J. L. (1960). Effect of a Partial Monolayer of Propping Agent on Fracture Flow Capacity.

Fredd, C. N., McConnell, S. B., Boney, C. L., England, K. W. (2001). "Experimental Study of Fracture Conductivity for Water-Fracturing and Conventional Fracturing Applications." SPE Journal 6(3): 288-298.

Grieser, B., Hobbs, J., Hunter, J., Ables, J. (2003). The Rocket Science Behind Water Frac Design. SPE Production and Operations Symposium. Oklahoma City, Oklahoma, Society of Petroleum Engineers Inc.

Lancaster, D. E., McKetta, S. F., Hill, R. E., Guidry, F. K., Jochen, J. E. (1992). Reservoir Evaluation, Completion Techniques, and Recent Results From Barnett Shale Development in the Fort Worth Basin. SPE Annual Technical Conference and Exhibition. Washington, D.C., 1992 Copyright 1992, Society of Petroleum Engineers Inc.

Makurat, A., Gutierrez, M. (1996). Fracture Flow and Fracture Cross Flow Experiments. SPE Annual Technical Conference and Exhibition. Denver, Colorado, 1996 Copyright 1996, Society of Petroleum Engineers, Inc.

Mayerhofer, M. J., Meehan, D. N. (1998). Waterfracs - Results from 50 Cotton Valley Wells. SPE Annual Technical Conference and Exhibition. New Orleans, Louisiana, 1998 Copyright 1998, Society of Petroleum Engineers Inc.

Mayerhofer, M. J., Richardson, M. F., Walker, R. N., Meehan, D. N., Oehler, M. W., Browning, R. R. (1997). Proppants? We Don't Need No Proppants. SPE Annual Technical Conference and Exhibition. San Antonio, Texas, 1997 Copyright 1997, Society of Petroleum Engineers, Inc.

Morales, R. H., Suarez-Rivera, R., Edelman, E. (2011). Experimental Evaluation of Hydraulic Fracture Impairment In Shale Reservoirs, American Rock Mechanics Association.

Olsson, W. A., Brown, S. R. (1993). "Hydromechanical response of a fracture undergoing compression and shear." International Journal of Rock Mechanics and Mining Sciences & Geomechanics Abstracts 30(7): 845-851.

Palisch, T. T., Vincent, M. C., Handren, P. J. (2010). "Slickwater Fracturing: Food for Thought." SPE Production & Operations 25(3): pp. 327-344.

Papazis, P.K.: 2005. Petrographic Characterization of the Barnett Shale, Fort Worth Basin, Texas. MS Thesis. The University of Texas at Austin, Austin, Texas.

Penny, G. S. (1987). An Evaluation of the Effects of Environmental Conditions and Fracturing Fluids Upon the Long-Term Conductivity of Proppants. SPE Annual Technical Conference and Exhibition. Dallas, Texas, 1987 Copyright 1987, Society of Petroleum Engineers.

Ramurthy, M., Barree, R. D., Kundert, D. P., Petre, E., Mullen, M. (2011). Surface Area vs Conductivity Type Fracture Treatments in Shale Reservoirs. SPE Hydraulic Fracturing Technology Conference. The Woodlands, Texas, USA, Society of Petroleum Engineers.

Rivers, M., Zhu, D., Hill, A. D., (2012). Proppant Fracture Conductivity With High Proppant Loading and High Closure Stress. SPE Hydraulic Fracturing Technology Conference. The Woodlands, Texas, USA, Society of Petroleum Engineers.

Schein, G. W., Carr, P. D., Canan, P. A., Richey, R. (2004). Ultra Lightweight Proppants: Their Use and Application in the Barnett Shale. SPE Annual Technical Conference and Exhibition. Houston, Texas, Society of Petroleum Engineers.

Walker, R. N. J., Hunter, J. L., Brake, Al C., Fagin, P. A., Steinsberger, N. (1998). Proppants, We Still Don't Need No Proppants - A Perspective of Several Operators. SPE Annual Technical Conference and Exhibition. New Orleans, Louisiana, 1998 Copyright 1998, Society of Petroleum Engineers Inc.

Warpinski, N. R., Du, J., Zimmer, U. (2012). Measurements of Hydraulic-Fracture-Induced Seismicity in Gas Shales. SPE Hydraulic Fracturing Technology Conference. The Woodlands, Texas, USA, Society of Petroleum Engineers.